International Journal of Fracture **95:** 103–141, 1999.

Size effect on compression strength of fiber composites failing by kink band propagation

ZDENĚK P. BAŽANT[1], JANG-JAY H. KIM[2], ISAAC M. DANIEL[3], EMILIE BECQ-GIRAUDON[4] and GOANGSEUP ZI[4]
[1]*Walter P. Murphy Professor of Civil Engineering and Materials Science, Northwestern University, Evanston, Illinois 60208; e-mail: z-bazant@nwu.edu.*
[2]*Graduate Research Assistant, Northwestern University; currently Research Engineer, Sandia National Laboratories, Albuquerque, New Mexico*
[3]*Walter P. Murphy Professor of Civil and Mechanical Engineering, Northwestern University.*
[4]*Graduate Research Assistant, Northwestern University.*

Received 16 July 1998; accepted in revised form 31 December 1998

Abstract. The effect of structure size on the nominal strength of unidirectional fiber-polymer composites, failing by propagation of a kink band with fiber microbuckling, is analyzed experimentally and theoretically. Tests of novel geometrically similar carbon–PEEK specimens, with notches slanted so as to lead to a pure kink band (not accompanied by shear or splitting cracks), are conducted. They confirm the possibility of stable growth of long kind bands before the peak load, and reveal the existence of a strong (deterministic, non-statistical) size effect. The bi-logarithmic plot of the nominal strength (load divided by size and thickness) versus the characteristic size agrees with the approximate size effect law proposed for quasibrittle failures in 1983 by Bažant. The plot exhibits a gradual transition from a horizontal asymptote, representing the case of no size effect (characteristic of plasticity or strength criteria), to an asymptote of slope $-\frac{1}{2}$ (characteristic of linear elastic fracture mechanics, LEFM). A new derivation of this law by approximate (asymptotically correct) J-integral analysis of the energy release, as well as by the recently proposed nonlocal fracture mechanics, is given. The size effect law is further generalized to notch-free specimens attaining the maximum load after a stable growth of a kink band transmitting a uniform residual stress, and the generalized law is verified by Soutis, Curtis and Fleck's recent compression tests of specimens with holes of different diameters. The nominal strength of specimens failing at the initiation of a kink band from a smooth surface is predicted to also exhibit a (deterministic) size effect if there is a nonzero stress gradient at the surface. A different size effect law is derived for this case by analyzing the stress redistribution. The size effect law for notched specimens permits the fracture energy of the kink band and the length of the fracture process zone at the front of the band to be identified solely from the measurements of maximum loads. The results indicate that the current design practice, which relies on the strength criteria or plasticity and thus inevitably misses the size effect, is acceptable only for small structural parts and, in the interest of safety, should be revised in the case of large structural parts.

Key words: Fracture, compression, fiber composites, testing, kink bands, microbuckling, size effect, scaling, asymptotic analysis, J-integral, equivalent LEFM, cohesive crack model.

1. Introduction

In the early 1980's it became clear that the size effect on the nominal strength of quasibrittle materials failing after large stable crack growth is caused principally by energy release (Bažant 1984) and cannot be explained by Weibull-type statistics of random microdefects. Ever since, the problem of size effect has received increasing attention (see the reviews in Bažant and Chen, 1997, and Bažant and Planas, 1998). Size effects caused by energy release

into a finite-size FPZ (or damage localization zone) have been extensively demonstrated and mathematically described for concrete, mortar, rocks, ceramics and sea ice. Description of such a size effect requires an energy analysis of fracture mechanics type.

At present, all the textbooks and practical procedures for fiber composites characterize the failure in terms of strength or plasticity type criteria, which are inherently incapable of capturing the size effect. Recently, though, the existence of size effect has been demonstrated by tests of notched orthotropic and quasi-isotropic carbon-epoxy laminates under tensile (Mode I) loading (Bažant, Daniel and Li, 1996). A size effect of thickness in laminates was experimentally shown by Daniel and Hsiao (1996).

The present study will focus attention on the compression failure of unidirectionally reinforced fiber composites. This is a particularly complex type of material failure, which can involve two distinct mechanisms:

(1) delamination fracture, and
(2) a row of parallel axial shear cracks combined with microbuckling of fibers in a so-called kink band.

Only the latter mechanism of failure will be considered in this study.

Compression microbuckling in kink bands has been studied extensively for over thirty years and a large body of knowledge has been accumulated. Rosen (1965) presented a simple formula for compression strength based on the idea of buckling of parallel fibers embedded in an elastic matrix. Similar more refined formulae for elastic composites with wavy fibers were presented by Bažant (1968). Argon (1972) extended Rosen's formula by considering plastic yielding.

A further important refinement was introduced by Budiansky (1983) who took into account the initial misalignment of the axial fibers and showed its pronounced effect. Various subsequent refinements within the framework of elastoplastic analysis were made by Budiansky and Fleck (1993), Kyriakides et al. (1995), Christensen and DeTereza (1997), Soutis et al. (1991, 1993), Moran et al. (1995), Jelf and Fleck (1992), Fleck and Jelf (1995), Fleck and Shu (1995), Fleck et al. (1996), Kyriakides and Ruff (1997), and others; see the excellent reviews by Fleck (1997), Budiansky and Fleck (1994), Schultheisz and Waas (1996), Waas and Schultheisz (1996), and Sutcliffe and Fleck (1994). These studies included the analysis of post-buckling behavior of the fibers, inelastic behavior of matrix, and various imperfections. They provided understanding of the factors governing the inclination of the kink band with regard to the direction of the fibers, including the role of lateral expansion in the kink band and the shape of the assumed yield surface. Analysis of microbuckle initiation by small-scale yielding fracture mechanics was presented by Sutcliffe et al. (1996)

None of the existing formulae for the nominal strength in compression, however, predicts any size effect. Omission of the size effect in compression has seemed natural because small-scale laboratory tests indicated no size effect and because the maximum load has been thought to occur at the very beginning of microbuckling, before the size or the length of the kink band becomes macroscopically significant.

Recently, though, various fracture mechanics aspects of the kink band failure came to light. Based on strain measurements at the flank of the kink band, the experimental studies of Sutcliffe and Fleck (1994) and Fleck et al. (1996, 1997) demonstrated that the axial normal stress across the band decreases with the distance from the band front, and reaches a plateau equal to about 50 percent of the maximum stress. This means that the diagram of the axial normal stress versus the axial relative displacement across the band exhibits softening and

then reaches a yield plateau at about 50 percent stress reduction. Such a crack-like behavior of the band (Fleck et al., 1996) was further confirmed by the study of Moran et al. (1995), who discovered the phenomenon of band broadening. In retrospect, the band broadening appears natural to expect because it is required to accommodate the increase of relative displacement across the band with the distance from the front, similar (but opposite in sign) to the increase of crack opening.

Fleck (1996) and Sutcliffe and Fleck (1996) conducted two-dimensional fracture analyses, adapting the cohesive crack model for compression, and estimated the fracture energy associated with the kink band propagation. Soutis et al. (1991) reported extensive numerical studies with a crack-bridging model and analyzed the effect of the size of a hole on the strength of a composite specimen. They calculated and experimentally verified how the apparent strength in the vicinity of a hole decreases with an increasing diameter of the hole. Although geometric similarity of the hole with the specimen dimensions was not maintained in these tests, the results nevertheless hint at the likelihood of size effect.

Recently, Budiansky, Fleck and Amazigo (1997) analyzed the propagation of a semi-infinite out-of-plane kink band, approximating the band with a crack whose face is allowed to overlap in compression. They assumed the FPZ to be lumped into a point, and analyzing energy balance derived the formula

$$\sigma_u = \sigma_b + \sqrt{G_b/L} \tag{1}$$

in which σ_u = axial normal stress 'upstream' in the direction of propagation (far enough ahead of the front), σ_b = axial normal stress transmitted across the band far enough behind the front, L = specimen height, and G_b = material constant playing the role of fracture energy and consisting of the work of sliding shear stresses in the band, the work of fiber debonding, and the work of the axial normal stress on the relative displacement across the band. Sutcliffe et al. (1996) examined the energy release rate required for microbuckle initiation by small-scale yielding fracture mechanics approach. required for microbuckle initiation

Although this formula does not give the effect of size L on the nominal strength of geometrically similar specimens and does not take into account the effect of the size of the FPZ at the front of the kink band, it clearly suggests the existence of a size effect. More importantly, the type of analysis that has led to this formula gives an inspiration for taking a fracture mechanics approach.

The present study, involving specimens of geometrically similar shapes, reports experimental results that reveal the existence a size effect in kink band compression failure and permit an approximate calibration of size effect theory. A simplified analysis of the energy release, briefly outlined at a recent conference (Bažant 1998(a)), is used to obtain closed-form formulae for the size effect in failures that occur either after a large stable growth of kink band, or at the initiation of the kink band. These formulae represent a special application of the general asymptotic analysis of size effect proposed for compression fracture in Bažant (1997) and Bažant and Chen (1997).

2. Size effect tests of notched specimens

The kink band failure is often combined with axial splitting-shear cracks and delaminations. Such combined failures are difficult to analyze because the contributions of the microbuckling in the kink band and of the shear, splitting and delamination failures are hard to separate.

Therefore, the objective of experimental investigation aimed at verifying a theory should be to find the type of fiber composite and the shape of specimen that would lead to a pure kink band failure and would do so even for very large sizes.

After experimenting with various types of composites, the carbon fiber composite with a PEEK (poly-ether-ether-keton) thermoplastic polymer matrix was selected. The advantage of PEEK is that it is less brittle than carbon epoxy composites, which leads to a more stable type of failure. It follows that, if a size effect is revealed in this type of composite, it should exist and be in fact more pronounced in more brittle composites, such as the carbon fiber-epoxy composites.

To exclude the effect of random variation of material strength over the specimen volume (known to cause Weibull-type size effect), the specimens (shown in Figure 1(a,c) and 2) need to be provided with notches. The notches ensure the failure to begin in one desired place, preventing the failure from starting at diverse locations where the material is statistically weakest.

Why a one-sided notch, rather than two symmetric notches? The reason is that a bifurcation of the equilibrium path would have to be expected to occur, according to the analysis in Bažant and Cedolin (1991, Sec. 12.5). Symmetric growth of two interacting kink bands would surely represent an unstable path. The stable path is a one-sided growth of one kink band even if there are two notches.

Notches that are orthogonal to the surface have normally been used in fracture testing. At the beginning of this study, however, such notches were found to engender failures that begin by an axial splitting-shear crack (Figure 1(b)), which is only later followed by the development of an out-of-plane kink band. Such a band typically has a transverse inclination (such inclination was previously observed by Fleck et al. (1996), Sutcliffe and Fleck (1994), Kyriakides et al. (1995)). For this reason, the starter notch has been made inclined (Figure 1(c), 2) with the same angle as the out-of-plane kink band. This inclination was found by trial tests to be 25.4°. It made it possible to eliminate in most tests the axial splitting-shear cracks and thus obtain pure kink band failures.

The test specimens, shown in Figure 1(a,c) and 2, are scaled in two dimensions. the thickness b in the third dimension being constant. The specimen dimensions and the notch depths of the specimens of different sizes are scaled in the ratio 1:2:4. The notch of length $a_0 = 0.3\,\mathrm{D}$, where D is the specimen width, is machined with a diamond bladed band saw up to 95 percent of its length. Then the notch is sharpened at the tip by a cut whose depth is 5 percent of the notch depth. The cut is machined with a 0.2 mm diameter diamond-studded wire, and thus the crack tip radius is 0.1 mm in all the specimens. The depth a_0 of the notch considered for scaling and in the analysis includes the depth of the wire saw cut.

The content of polymer resin in the specimen (supplied by Fiberite, Inc., Orange, California) was 32 ± 3 percent. The specimens have been molded at Northwestern University from 100 plies of sheets 304.8×304.8 mm, 0.05 mm thick. The molding was carried out under temperature 391°C (735°F) and pressure 0.69 MPa, using the standard time sequence of the curing process. After the specimens had been cut from the molded sheets, they were provided with massive end caps made of 1040 hot rod steel, to which they were glued by epoxy. To ensure proper alignment, the end caps were glued only after the specimen had been installed under the loading platens of the testing machine. The end plates were restrained to prevent any rotations. All the specimens have been tested under a controlled stroke rate of 1.27×10^{-4} mm/s. After the kink band had initiated at the notch tip, it was seen to propagate stably on both the front and back sides of the specimen. On one side, the kink band was usually

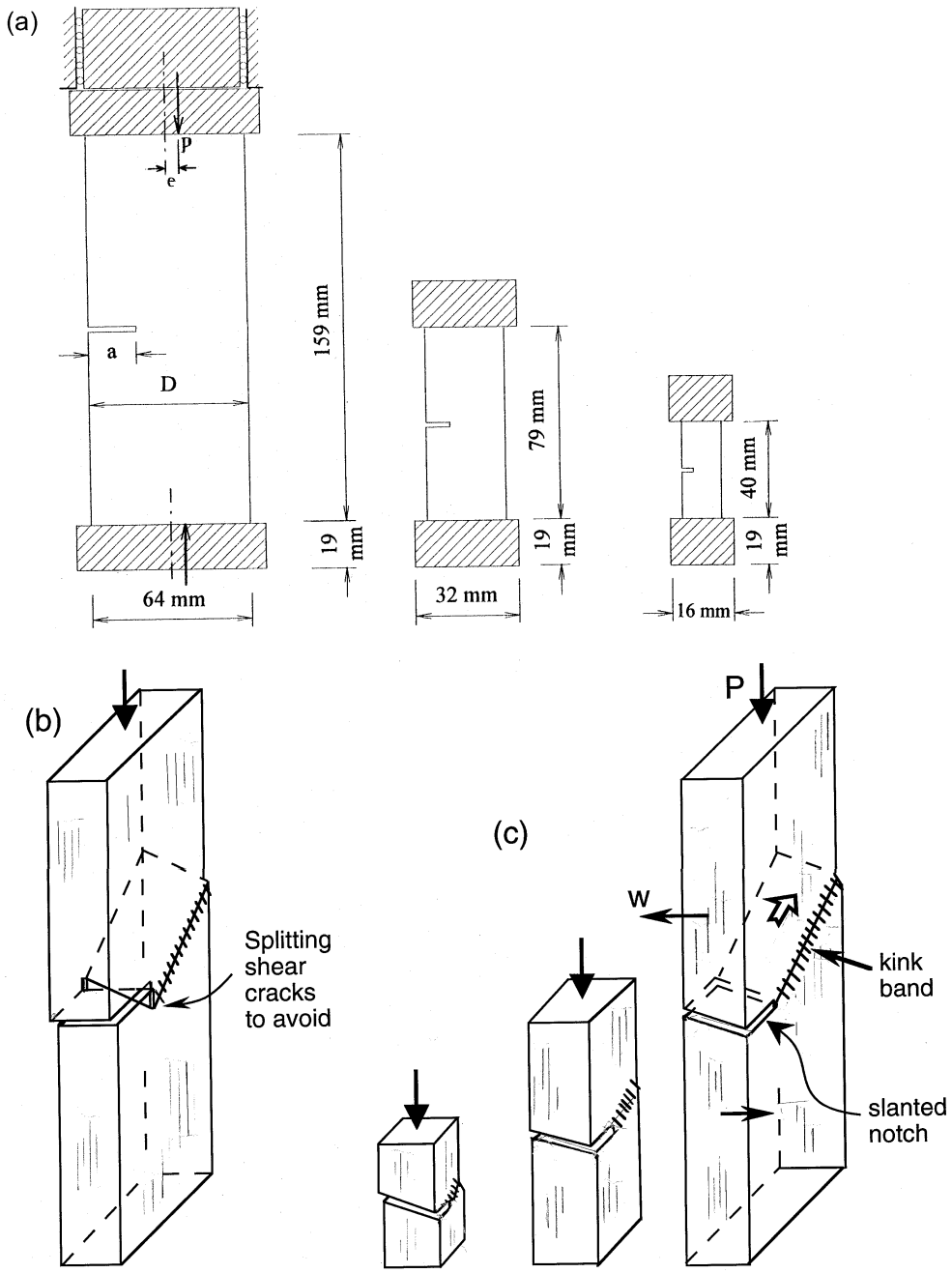

Figure 1. (a) Geometrically similar single-edge notched carbon-PEEK (poly-ether-ether-keton) specimens tested, and scheme of loading, (b) specimen with an orthogonal notch exhibiting undesirable failure (splitting-shear cracks), and (c) transversely slanted notches used in present tests (Figures 3 and 4), achieving pure kink band failure.

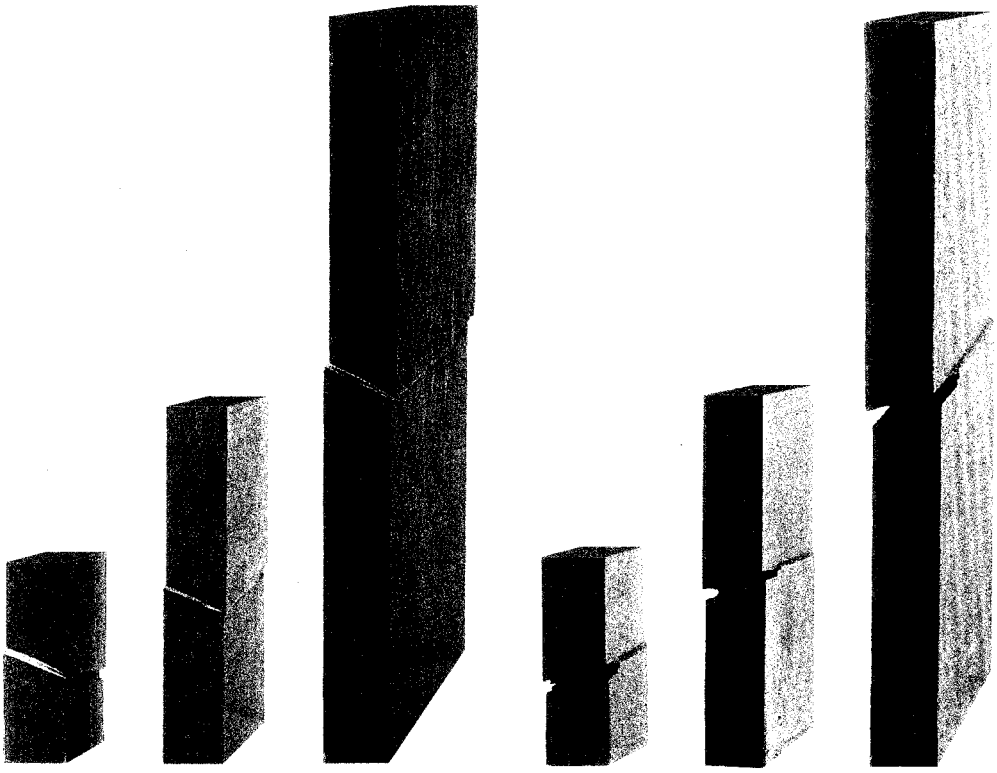

Figure 2. Photo of three of the specimens after the test, showing the out-of-plane kink band.

slightly longer than on the other side, but only at the beginning of propagation. The shorter band on one side would soon catch up with the longer band on the opposite side.

As usual, the nominal strength of the specimen, which represents a parameter of the maximum load having the dimension of stress, is defined as

$$\sigma_N = P/bD, \tag{2}$$

in which P = maximum load measured, b = specimen thickness (12.7 mm (0.5 in)), and D = specimen width (chosen as the characteristic dimension). Figure 3 shows the individual test results in the form of the plot of $\log \sigma_N$ versus $\log D$.

Figure 4 further shows for the individual specimens the diagrams of the measured average stress over the ligament, $\sigma_L = \sigma_N D/(D - a_0)$, versus the average axial strain $\overline{\varepsilon}$ determined as the stroke of the piston divided by the length between the platens. All these load-deflection diagrams exhibit a post-peak stress drop rather than a horizontal yield plateau at peak load. This fact alone suffices to demonstrate that a fracture-type approach (or a nonlocal damage approach) is required. Furthermore, these diagrams reveal the existence of a terminal yield plateau, which confirms the existence of a finite residual stress across the kink band.

If there were no size effect, as currently assumed in design and exhibited by the existing formulae for the maximum load expressed in terms of stress or strain, the plot in Figure 3 would have to be horizontal. Every theory based on plasticity or on some critical values of stress or strain predicts a horizontal plot. However, the trend is clearly seen to be downward. The downward slope is quite steep and closer to the slope $-\frac{1}{2}$ corresponding to LEFM than

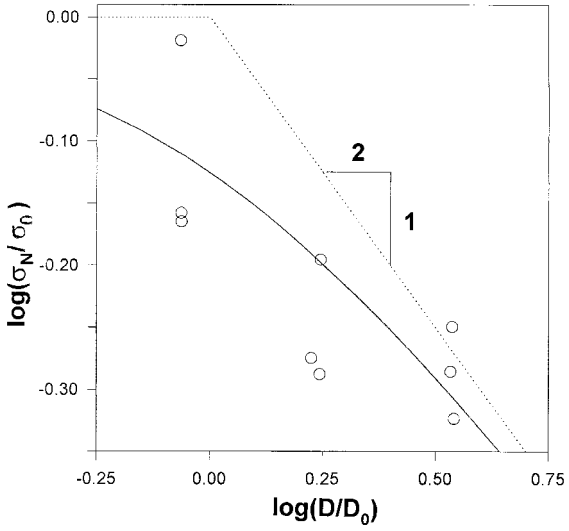

Figure 3. Results of the present tests of nominal strength of carbon-PEEK specimens (data points) and their optimum fit by equation (14).

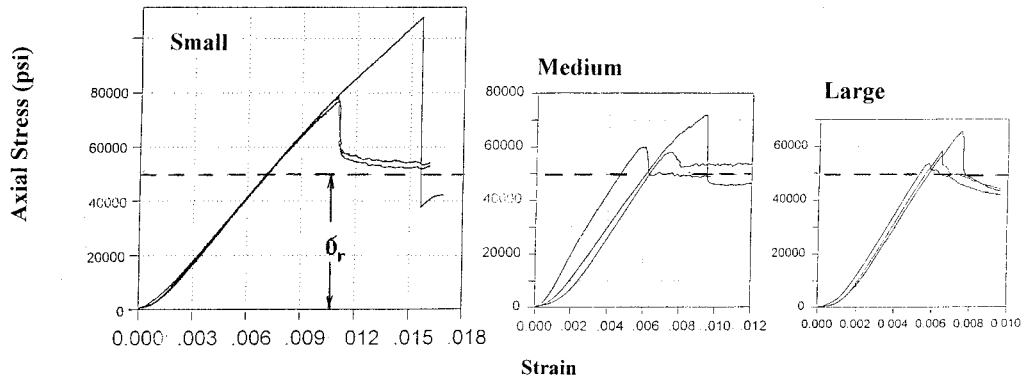

Figure 4. Load-deflection diagrams of carbon-PEEK specimens tested.

to the horizontal line for the strength theory. So, despite a relatively ductile PEEK matrix, the size effect for these large, albeit not extremely large, specimens is strong.

One of the small specimens, corresponding to the upper left data point in Figure 3, did not develop a kink band but failed by a vertical shear crack that started from the notch tip and produced axial splitting. Argued though it could be that this data point should be excluded, it has nevertheless been retained in the data set, because

(1) it is the highest point in the data set, and
(2) the load that would cause the kink band failure of this specimen must have been at least as high as this point.

In other words, the size effect could not be milder than it is when this point is included in the analysis.

The test results exhibit considerable random scatter. This is, however, typical of compression failure of fiber composites (because of their strong sensitivity to fiber misalignment;

Fleck 1997, Budiansky 1983). For this reason, the size effect would not have been revealed clearly if the size range were less than 1:4. The present size range of 1:4 appears just about the minimum for being able to clearly demonstrate the size effect. To reduce the ratio of the inevitable scatter band width to the range of sizes, the ratio of the sizes of the smallest and largest specimens should be at least 1:8 in future testing. For concrete, tests with size ranges up to 1:32 have been made (Bažant and Planas 1998). For sea ice, tests of a size range of 1:162 have been carried out by Dempsey's team in the Arctic Ocean (Dempsey et al., 1999), providing a clear picture of the size effect despite strong random scatter.

Compared to the loading through a pin, which would allow free rotations at the ends, the present boundary condition of restraint against rotation complicates a little bit the test evaluation because an unknown bending moment develops at the ends causing the compression resultant to shift laterally during kink band propagation. However, the end restraint has the advantage that the test becomes much more stable. This has made it possible to

(1) demonstrate that a stable propagation of a long kink band is possible (which has so far been doubted by most experts),
(2) observe the post-peak deformations well beyond the peak load, and
(3) approach the residual stress plateau and observe the residual stress (Figure 4).

3. Simple size effect analysis via J-integral

We analyze a specimen (Figure 5(a)) with unidirectional (axial) fiber reinforcement. The kink band has length a which can be long or short compared to the specimen width D taken as the characteristic dimension. The width of the kink band, considered to be small, is denoted as w, and its inclination as β (Figure 5(a), 6). Although tractable, the bending stiffness of the fibers is neglected, for the sake of simplicity. The loading is assumed to produce cohesive shear cracks that are parallel to the fibers and have a certain characteristic spacing s. The axial normal stress transmitted across the kink band (band-bridging stress) is denoted as σ (Figure 6). Although Figure 5(a) depicts an in-plane fiber inclination, the behavior is similar for the out-of-plane fiber inclination in the test specimen used because what matters for the analysis is the reduction of axial stress across the kink band, which is the same for both cases.

The diagram of the shear stress τ transmitted across the shear cracks versus the slip displacement η_{fr} on these cracks must exhibit post-peak softening (Figure 7 top left). This is confirmed by two important recent experimental findings. First, Fleck and Shu (1995) placed strain gauges at the flanks of the kink band and, as the kink band grew, observed the strain in the gages to decrease, rather remain constant (see also Fleck, 1997). Second, Moran et al. (1995) recently discovered the phenomenon of band broadening (see also Sutcliffe et al., 1996), which implies that the relative displacement across the band increases as the band grows, and thus indicates that the kink band plays a role similar to a crack (whose opening width grows with the distance from the front and the transmitted stress decreases), rather than to a dislocation line (on which the relative displacement as well as the transmitted stress remains constant).

For the sake of simplicity, the stress-displacement diagram of the axial shear cracks is considered to be bilinear, as shown in Figure 7 (top right) where τ_p = peak stress or shear strength = shear stress parallel to fibers at which the cohesive crack initiates, and τ_r = the residual shear strength, representing the final yield plateau. According to the analysis of mode II slip bands by Palmer and Rice (1973), the area of the diagram above the yield plateau is

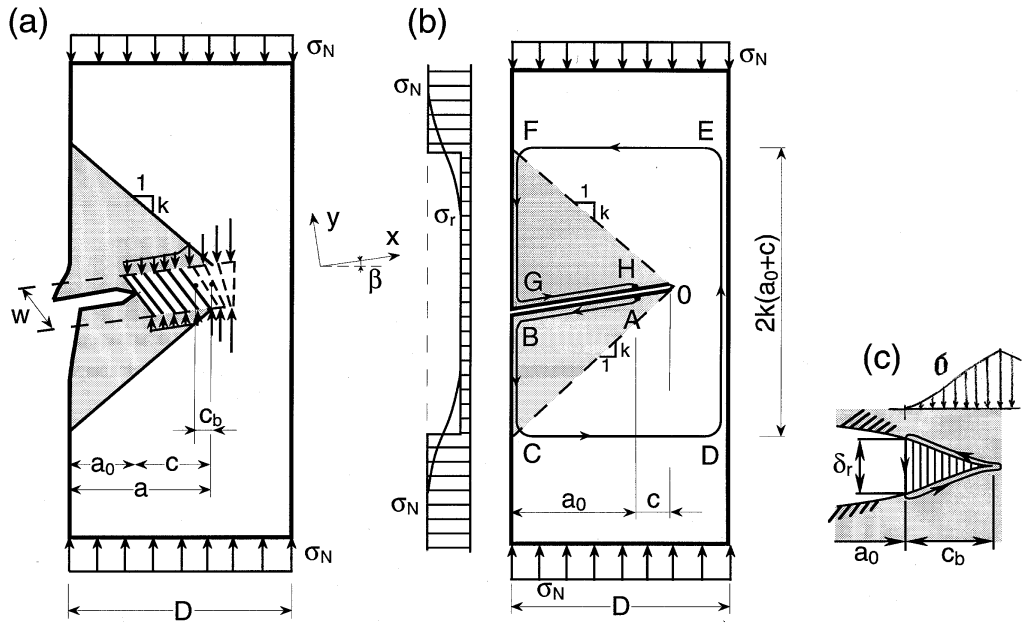

Figure 5. (a) Idealized kink band of width w in a notched specimen, with a fracture process zone of effective length c_b; (b) path of J-integral, with energy release (stress relief) zones OFGO, OBCO; (c) fracture process zone of equivalent cohesive crack.

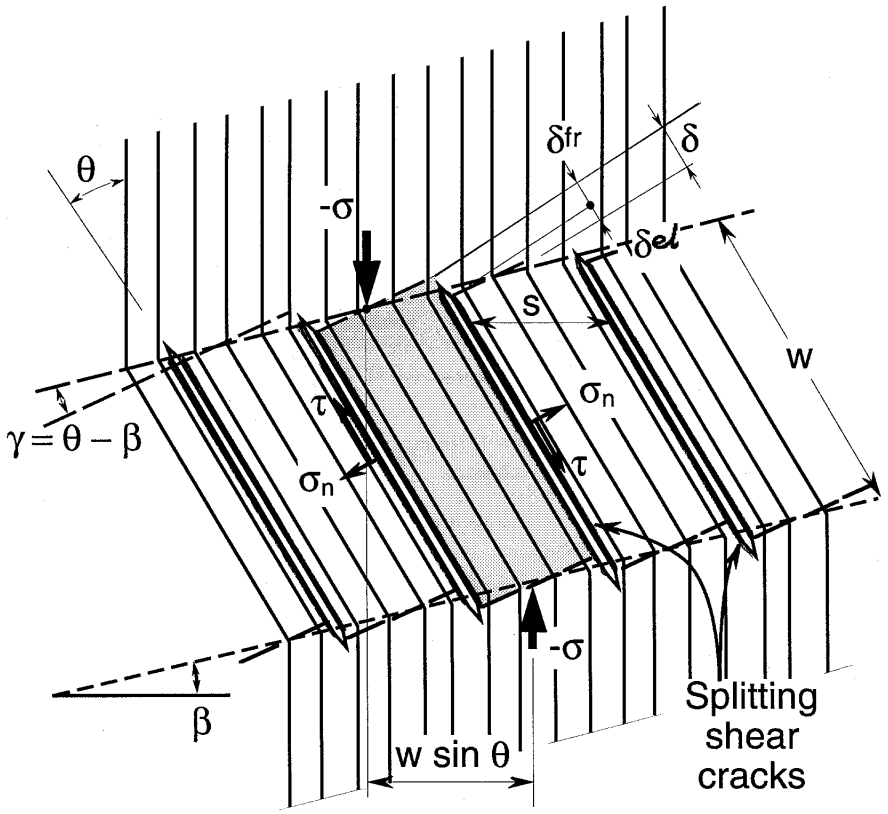

Figure 6. Idealized microbuckling of fibers in the kink band and axial shear cracks.

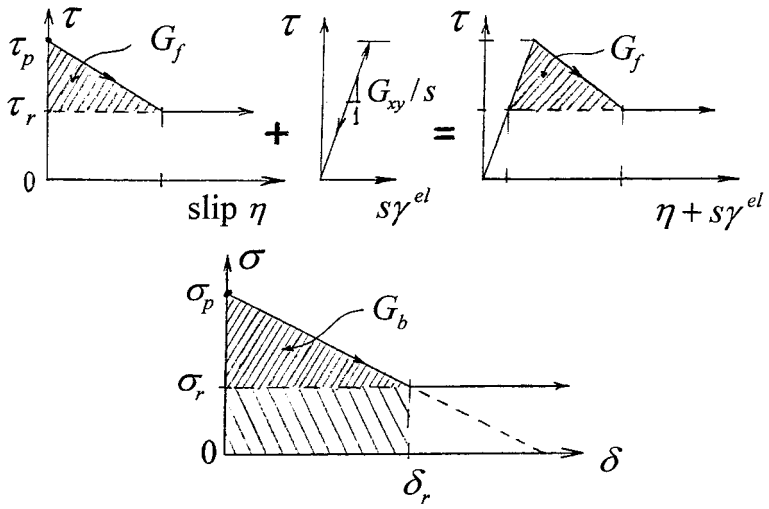

Figure 7. Top left: assumed bilinear diagram of shear stress versus slip displacement on the axial cracks of spacing s, crossing the kink band. Top right: superposition of elastic deformation between the cracks to obtain the diagram of shear stress versus total shear displacement accumulated over distance s between cracks. Bottom: Diagram of the axial normal stress σ versus axial displacement δ across the kink band, and area representing the kink band fracture energy G_b.

known to play the role of shear (Mode II) fracture energy, G_f (see the shaded triangle in Figure 7 top left) (the critical value J_{cr} of the J-integral also includes the rectangle below the triangle). The fracture energy of the kink band, that is, the energy dissipated by fracture per unit length of the band, is

$$G_b = G_f w / s. \tag{3}$$

3.1. J-INTEGRAL CALCULATIONS

To approximately calculate the energy release due to propagation of the kink band, we use Rice's (1968a) J-integral, for which we consider the rectangular closed path $ABCDEFGH$ shown in Figure 5(b). The start and the end of this path at the crack surfaces must lie at the boundary of the FPZ because the residual stress across the band does work (for Mode II cracks this was shown by Palmer and Rice, 1973). The top, bottom and right sides of this rectangular path, $CDEF$, are sufficiently remote from the crack band for the initially uniform stress state to remain undisturbed.

On the left downward sides of the rectangular path, FG and BC, the distribution of the axial stress has some curved profile sketched on the left of Figure 5(b). The precise shape of this profile is not important but it is important that asymptotically, for large sizes $D \gg w$, the profiles must become geometrically similar. This observation is the basic idea of the asymptotic size effect analysis via the J-integral.

For the sake of simplicity, we may replace this profile by the stepped piece-wise constant profile shown, in which the stress drops abruptly from the initial stress σ_N to the residual stress σ_r which is transmitted across the band after the band contracts sufficiently. An important point again is that, for large enough geometrically similar specimens ($D \gg w$), the locations of the stress steps in this replacement profile must also be similar, that is, points F and C,

must lie on inclined rays of a certain constant slope k shown dashed in Figure 5(b). These rays may be imagined to emanate from the tip of the equivalent crack of length $a = a_0 + c_b$ (Figure 5(b)) where c_b characterizes the length of the FPZ of the kink band and represents approximately the distance from the center of the FPZ of kink band to the point where the stress is reduced to its residual value σ_r (Figure 7 top; the length of the FPZ is about $2c_b$). Slope k depends on the structure geometry and on the orthotropic elastic constants.

The area between these rays and the kink band roughly represents the zone of stress relief caused by the drop of axial stress transmitted by the kink band. The strain energy contained within this area is released and is dissipated by the axial shear cracks forming at the front of the kink band. Noting that this area, and thus the energy release, increases in proportion to D^2, while the energy dissipated at the kink band front increases linearly with D, one immediately concludes that there must be size effect.

The zone at kink band front in which the axial shear cracks are forming represents the FPZ of the kink band. Its length c_b may be regarded as a material property, almost independent of the specimen dimensions and geometry. It may be considered to be of the same order of magnitude as the width w. Throughout this zone, the fiber inclination increases from the initial misalignment angle $\overline{\varphi}$ up to the value $\overline{\varphi} + \varphi$ corresponding to the residual cracks. To make test evaluation simple, the specimens must be notched and the FPZ at maximum load must still be attached to the notch (i.e. $c = c_b$).

Referring to the sketch in Figure 5(b), the crack band of length $a_0 + c_f$ is approximately equivalent to a mode I crack whose faces are imagined to interpenetrate. The length of this crack is $a_0 + c$ where $c = c_f + (w/2k)$, which may again be assumed to be approximately a constant when the size is varied. Consequently, the height FC of the rectangular path in Figure 5b is approximately $2k(a_0 + c)$, as labeled in the figure.

In view of these considerations, the first part of the J-Integral may be approximately expressed as follows

$$\oint \overline{W}\,\mathrm{d}y = 2k(a_0 + c)\left(\frac{\sigma_N^2}{2E_y} - \frac{\sigma_r^2}{2E_y}\right), \tag{4}$$

in which $\overline{W}$ = strain energy density, and y = coordinate normal to the direction of propagation (Figure 5(b)), and E_y = effective elastic modulus of the orthotropic fiber composite in the fiber direction y (with different values for plane strain and plane stress). In (4) we have considered that the parts of the integral over the horizontal segments are 0, and that the stress on the vertical segment DE may be assumed undisturbed by the kink band, i.e., equal to σ_N. The portions of the integral over the crack surface segments GH and AB are, likewise, 0.

The second part of the J-Integral may be calculated in a similar manner as that introduced by Palmer and Rice (1973) for the propagation of Mode II shear fracture with residual friction;

$$\begin{aligned}\oint \boldsymbol{\sigma} \cdot \frac{\partial \boldsymbol{u}}{\partial x}\,\mathrm{d}x &= \int_{AB} \sigma_r \frac{\mathrm{d}}{\mathrm{d}x}\left[\frac{1}{2}\delta(x)\right]\mathrm{d}x - \int_{GH} \sigma_r \frac{\mathrm{d}}{\mathrm{d}x}\left[\frac{1}{2}\delta(x)\right]\mathrm{d}x \\ &= \int_{x=0}^{a_0} \sigma_r\,\mathrm{d}\delta(x) = \sigma_r \int_{x=0}^{a_0} \mathrm{d}\delta(x) = \sigma_r \delta_{BG},\end{aligned} \tag{5}$$

in which $\boldsymbol{\sigma}$ = stress vector acting from the outside on the domain enclosed by the path, $\boldsymbol{u}$ = displacement vector, δ = relative displacement across the band, and δ_{BG} = relative displacement between points B and G. That displacement can be estimated as the difference

between the changes of length $\overline{ED}$ and length $\overline{FC}$;

$$\delta_{BG} = \Delta\overline{ED} - \left(\Delta\overline{FG} + \Delta\overline{BC}\right) \tag{6}$$

$$= 2k\,(a_0 + c)\,\frac{\sigma_N}{E_y} - 2k\,(a_0 + c)\,\frac{\sigma_r}{E_y} = 2k\,(a_0 + c)\,\frac{\sigma_N - \sigma_r}{E_y}. \tag{7}$$

Now the J-Integral may be readily evaluated as follows:

$$J = \oint \left(\overline{W}\,\mathrm{d}y - \boldsymbol{\sigma} \cdot \frac{\partial \boldsymbol{u}}{\partial x}\,\mathrm{d}s\right) = \frac{k}{E_y}\,(a_0 + c)\left[\sigma_N^2 - \sigma_r^2 - 2(\sigma_N - \sigma_r)\sigma_r\right]$$

$$= \frac{k}{E_y}\,(a_0 + c)\,(\sigma_N - \sigma_r)^2 \tag{8}$$

The energy consumed may be calculated again with the help of the J-Integral. Similar to Rice (1968b) and Palmer and Rice (1973), the integration path that runs along the equivalent crack surface and around the crack tip (Figure 5(c)) may be used;

$$J_{\mathrm{cr}} = \oint \boldsymbol{\sigma} \cdot \frac{\partial \boldsymbol{u}}{\partial x}\,\mathrm{d}x. \tag{9}$$

This represents the critical value J_{cr}, of the J-Integral required for propagation. This critical value may be subdivided into two terms

$$J_{\mathrm{cr}} = G_b + \sigma_r \delta_r \tag{10}$$

where G_b is the fracture energy, i.e., the energy required to produce the axial shear cracks across the kink band, and $\sigma_r \delta_r$, represents the plastic work that is done by the residual stresses σ_r within the FPZ of the kink band and is leaving the FPZ in its wake. This work corresponds in Figure 7 (top left) to the shaded rectangle lying under the shaded triangle. Following the way shown by Rice (1968b) and Palmer and Rice (1973) for shear bands, J_{cr} may be evaluated (Figure 5(c)) as follows

$$J_{\mathrm{cr}} = \oint \boldsymbol{\sigma} \cdot \frac{\partial \boldsymbol{u}}{\partial x}\,\mathrm{d}x$$

$$= -\int_{x=a_0}^{a_0+c} f[\delta(x)]\frac{\mathrm{d}}{\mathrm{d}x}[\tfrac{1}{2}\delta(x)]\,\mathrm{d}x + \int_{x=a_0+c}^{a_0} f[\delta(x)]\frac{\mathrm{d}}{\mathrm{d}x}[\tfrac{1}{2}\delta(x)]\,\mathrm{d}x$$

$$= -\int_{x=a_0}^{a_0+c} f[\delta(x)]\frac{\mathrm{d}\delta(x)}{\mathrm{d}x}\,\mathrm{d}x = \int_0^{\delta_r} f[\delta(x)]\,\mathrm{d}\delta(x). \tag{11}$$

This means that J_{cr} represents the sum of the shaded triangle and shaded rectangle in the stress-displacement diagram of Figure 7 (bottom). Therefore, according to (10), fracture energy G_b is represented by the area under the descending stress-displacement curve and above the horizontal line for the residual stress.

3.2. CASE OF LONG KINK BAND

Setting (8) equal to (10), and solving for the nominal strength σ_N of the specimen, we obtain

$$\sigma_N = \sigma_R + \sqrt{\frac{E_y(G_b + \sigma_r\delta_r)/kc}{1 + D/D_0}} = \sigma_R + \frac{\sigma_0}{\sqrt{1 + D/D_0}}, \tag{12}$$

in which

$$D_0 = \frac{c}{\alpha_0}, \qquad \sigma_0 = \sqrt{\frac{E_y(G_b + \sigma_r\delta_r)}{kc}}, \qquad \alpha_0 = \frac{a_0}{D}, \qquad \sigma_R = \sigma_r \tag{13}$$

(for other geometries, σ_R need not be equal to σ_r). The resulting formula (12) has the same form as that proposed by Bažant (1987) for the general case of quasibrittle failures with a residual plastic mechanism, and subsequently verified for several applications to concrete structure. This formula is valid when a long enough kink band transmitting constant residual stress σ_r develops in a stable manner before the maximum load is reached. Because of σ_r, such stable propagation can happen even in specimens of positive geometry (i.e., for increasing $g(\alpha)$). Stable propagation is helped by rotational restraint of specimen ends.

Equation (12) with (13) bears some similarity to formula (1) derived by Budiansky, Fleck and Amazigo (1997). In contrast to that formula, however, (12) with (13) describes the size effect for geometrically similar specimens, takes into account the finiteness of the FPZ at the front of the kink band, and involves a stress quantity of a different meaning (namely the nominal strength, which is a parameter of the applied load) instead of the stress values in front of the kink band and on its flanks.

3.3. FAILURE AT THE START OF KINK BAND FROM A NOTCH OR STRESS-FREE CRACK

In the case of notched test specimens (of suitable geometry), the maximum load is achieved while the FPZ of the kink band is still attached to the notch. Except for the sign of the band-bridging stresses, the situation is analogous to tensile fracture of notched specimens. From experiments on concrete as well as analytical studies based on the cohesive crack model, it is known that only a short initial portion of the softening stress-displacement curve of the cohesive crack comes into play. It is only the initial downward slope of this curve which matters for the maximum load (the tail of the postpeak load-deflection diagram, of course, depends on the entire stress-displacement curve of the cohesive crack); see Bažant and Li (1995) or Bažant and Planas (1998).

A similar situation must be expected for kink bands in notched specimens. Since the shape of the softening stress displacement curve of the cohesive crack model is irrelevant for the maximum load, except for the initial downward slope of the curve, the maximum load must be the same as that for a linear stress-displacement diagram, shown by the descending dashed straight line shown in Figure 7 (bottom).

It follows that in this case the residual stress σ_r should be disregarded and the fracture energy G_B that mathematically governs the kink band growth at maximum load of a notched specimen corresponds to the entire area under the extended descending straight line in Figure 7. Obviously, $G_B > G_b$ if $\sigma_r > 0$. Consequently, setting $\delta_r = 0$ in (13) and replacing G_b by G_B, we have the size effect law

$$\sigma_N = \frac{\sigma_0}{\sqrt{1 + D/D_0}}, \tag{14}$$

with

$$D_0 = \frac{c_0}{\alpha_0}, \qquad \sigma_0 = \sqrt{\frac{E_y G_B}{k c_0}}, \qquad c_0 = c_b + \frac{w}{2k}. \tag{15}$$

This coincides with the approximate size effect law proposed in Bažant (1983, 1984); Figure 8 (left, for $\sigma_R = 0$).

From experience with other materials, the length (at maximum load) of the crack band up to the beginning of the FPZ, a_0, may often be considered to be roughly proportional to the specimen size D, within a certain range of sizes. In other words, the ratio D/a_0 at maximum load of geometrically similar structures is often approximately constant. So is the value of D_0 in (14), provided that the specimens are geometrically similar.

3.4. Further considerations and generalization

The foregoing analysis is generally valid for any type of distributed or concentrated load applied on the top and bottom boundaries of the specimen, provided they are sufficiently remote. For the special case of a uniform load, the results can be more directly obtained by a simpler procedure that is based on the principle of superposition. As illustrated in Figure 9, the solution for a specimen with residual stress in the kink band consists of the solution of a specimen in which the distributed load at the top and bottom boundaries is equal to the residual stress (in which case the stress state is uniform, $\sigma = \sigma_r$) plus the solution of a specimen with a mode I stress-free crack loaded at top and bottom boundaries by $\sigma_N - \sigma_r$. In that case it suffices to take the J-integral only along the path $BCDEFG$, that is, omit the segments AB and HG along the crack surface. In such an approach, (5) vanishes. This leads directly to an expression of the type (14), but with $\sigma_N - \sigma_r$ on the left-hand side, which is evidently equivalent to (12).

In a complete analysis of the boundary value problem, the values of δ_c and of the kink band length are determined by the condition that the total stress intensity factor caused by the applied load and by the band-bridging stresses must vanish. As shown by Palmer and Rice (1973), by writing this conditions for the limiting case of an infinite body, an estimate of the length of the FPZ of the kink band can be obtained from the slope of the stress-displacement law of the cohesive shear cracks and their spacing s. From that length and the spacing, vice versa, one can obtain an estimate of the slope of the stress-displacement diagram.

Instead of expanding into Taylor series function $g(\alpha)$, it is equally justified to expand a power of $g(\alpha)$ as a function of a power of α. In this way (same as in Bažant 1997 or Bažant and Planas 1998, Eq. 9.1.34), one can show that (12) may be replaced by the following more general formula (Figure 8(a,b)):

$$\sigma_N = \sigma_R + \sigma_0 \left[1 + \left(\frac{D}{D_0}\right)^r\right]^{-1/2r}. \tag{16}$$

Exponent r, a constant, controls the curvature of the size effect plot in Figure 8 (left). The optimal value of r needs to be determined either experimentally or by some more refined theory (for concrete it is close to 1).

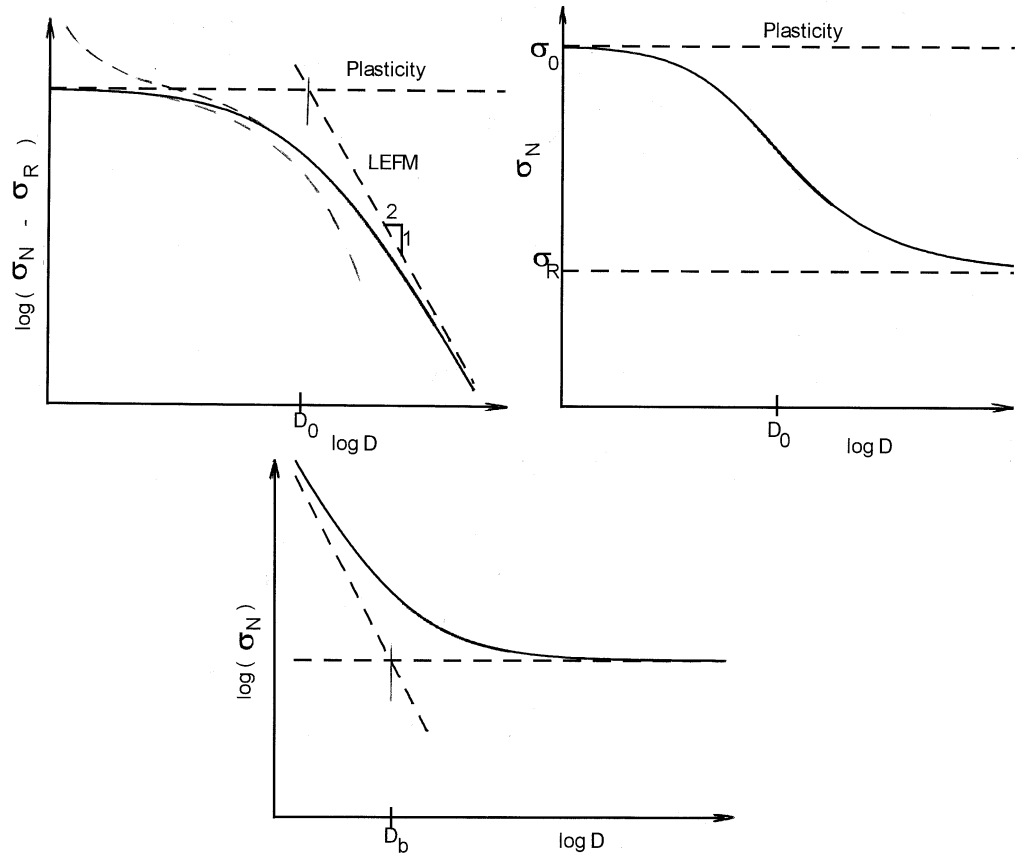

Figure 8. (a) Size effect law (solid curve) for specimens with a long kink band or notch (Eq.14) and asymptotic formulas (dashed curves). (b) Same but with σ_N instead of $\log \sigma_N$ as the ordinate). (c) Size effect law when $P_{\max}$ occurs at kink band initiation.

3.5. RESIDUAL STRENGTH OF SPECIMENS WITH NOTCH OR LONG KINK BAND

The residual stress in the kink band may be estimated by a simple extension of the formula presented by Budiansky (1983). From the moment equilibrium condition of an element of the kink band between two adjacent shear cracks (shaded, in Figure 6), we have $(\sigma s)(w \sin \vartheta) = (\tau w)s$, which expresses the second-order nonlinear geometric effect of buckling. Assuming the fiber inclination θ at the onset of the slip plateau to be small, we thus have the approximations $\sigma = \tau/\vartheta$ and $\sigma_r = \tau_r/\vartheta$.

The total rotation of the fibers in the kink band may be expressed as

$$\vartheta = \overline{\varphi} + \varphi + \frac{\delta}{s} = \overline{\varphi} + \frac{\tau_r}{G_{xy}} + \frac{\delta_f}{s}, \tag{17}$$

in which $\overline{\phi}$ = initial inclination angle of the fibers (an imperfection), G_{xy} = elastic shear modulus for planes parallel to the fibers, δ_f = slip displacement of the axial (shear) cracks

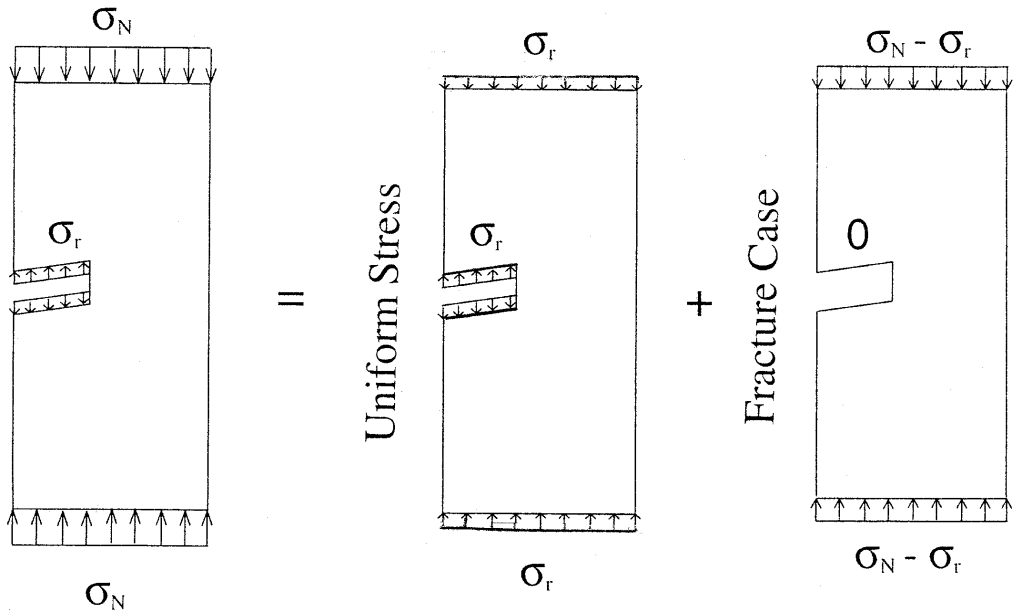

Figure 9. Application of principle of superposition to kink band with residual stress σ_r (the stress field in the middle specimen is uniform, $K_{\mathrm{I}} = 0$).

at the onset of the yield plateau (Figure 7), and ϕ = rotation of the fibers due to elastic shear deformation of the matrix in the kink band. From (17) it follows that

$$\sigma_r = \frac{\tau_r}{\vartheta} = \frac{\tau_r}{\overline{\varphi} + \frac{\tau_r}{G_{xy}} + \frac{\delta_f}{s}} = \frac{G_{xy}}{1 + \frac{\overline{\varphi} + (\delta_f/s)}{\varphi}}. \tag{18}$$

The last expression is the same as that obtained by Budiansky (1983) except for the additional term δ_f/s, which expresses the increase of the shear angle due to crack slip. Budiansky's formula of course refers to the maximum load (of a plastic kink band without fractures), whereas the present formula applies to the residual stress in the kink band after fracturing.

3.6. Case of kink band initiation from smooth surface

If there is no notch, the maximum load may often occur when the crack band initiates from a smooth surface. However, unless the size of the specimen is very large, a sizable FPZ, of a certain effective length c_b (Figure 10), must form at the kink band front before the maximum load is reached. This must evidently cause significant stress redistribution, which may be seen as the source of the size effect.

This type of size effect, observed in the bending tests of the modulus of rupture, is well documented and well understood for concrete and rocks. It can also be explained on the basis of energy release. In this case, however, one must take into account the second-order derivatives of the energy release rate because the energy release rate for an initiating crack or kink band, still infinitely short, is 0. The present simple approach is not accurate enough for determining these higher-order derivatives. Therefore, the size effect can be more conveniently and perhaps more instructively explained and quantified by analyzing the stress redistribution (as already done for concrete in Bažant and Li, 1995).

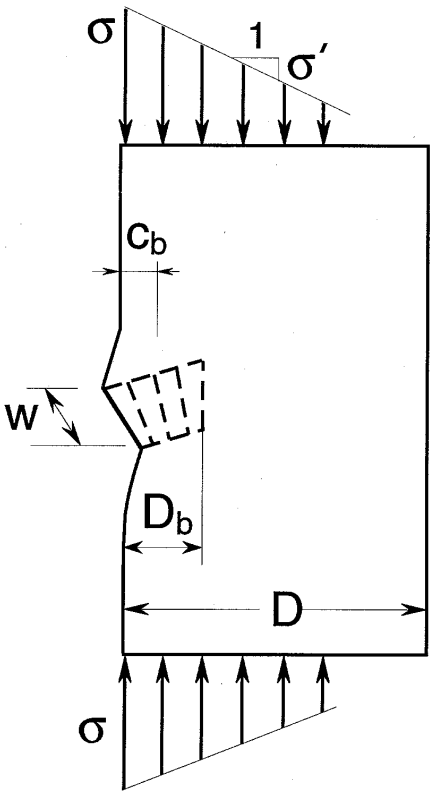

Figure 10. Kink band initiation from a smooth surface in a stress field with a stress gradient.

The size effect at crack initiation is known to occur only if the stress distribution has a significant stress gradient $\sigma_{,x}$ and reaches its maximum at the surface (Figure 10). The stress distribution near the surface is considered in the form

$$\sigma = \sigma_1 - \sigma_{,x}x = \sigma_N(1+\eta) - 2\eta\sigma_N\frac{x}{D}, \tag{19}$$

in which x = distance from the surface; $\sigma_1, \sigma_{,x}$ = values of the stress and its gradient at the surface ($x = 0$) before the kink band has formed. If the stress distribution is calculated from the theory of bending and is caused by axial load $P = \sigma_N bD$ of eccentricity e, then $\eta = 6e/D$ (dimensionless stress gradient).

A simple solution may proceed as follows. Based on the experience with the analysis of size effect on the modulus of rupture in other quasibrittle materials (Bažant and Li 1995), the stress under maximum load at the front of the FPZ, lying at distance $x = c_b$ from the surface (Figure 10), may be assumed to be equal to the strength limit σ_0 at which the kink band begins to form, which corresponds to the maximum stress point on the diagram of band-bridging stress versus contraction of the band; $[\sigma]_{x=c_b} = \sigma_0$ or

$$\sigma_N = \sigma_\infty/(1 - D_b/D), \tag{20}$$

in which

$$D_b = 2c_b\eta/(1+\eta), \qquad \sigma_\infty = \sigma_0/(1+\eta). \tag{21}$$

Equation (20) cannot be applied for $D \leqslant D_b$. But it so happens that the large-size approximation $(1 - D_b/D)^{-1} \approx 1 + D_b/D$ produces a formula that has the same large-size asymptotic behavior yet its behavior is also acceptable for the entire range of D

$$\sigma_N = \sigma_\infty \left(1 + \frac{D_b}{D}\right), \tag{22}$$

(Figure 8(c)). The values of σ_∞ and D_b are constants, the latter representing the thickness of the boundary layer in which the kink band damage takes place. For a vanishing stress gradient or a vanishing load eccentricity, one has $\eta = 0$, and the (deterministic) size effect then disappears.

Equation (22) is of the same form as previously derived for concrete (Bažant and Li, 1995, Bažant and Planas, 1997). One can also obtain the same equation by a more sophisticated analysis in which the stress redistribution due to the kink band is actually calculated and the maximum load is determined from the redistributed stresses (similar to Bažant and Li, 1995). Such an analysis could also be applied here, but it is more complicated. A still more rational approach is an asymptotic analysis based on the energy release functions of LEFM, which is outlined next.

Equation (22) is accurate only up to the first two terms of the asymptotic power series expansion of σ_N in $1/D$. This means that other formulae whose asymptotic expansion in $1/D$ coincides up to the first two terms with that of (22) are equally justified; for example

$$\sigma_N = \sigma_\infty \sqrt{1 + \frac{2D_b}{D}} \quad \text{or} \quad \sigma_N = \sigma_\infty \left(1 + \frac{q D_b}{D}\right)^{1/q}, \tag{23}$$

with any positive constant q.

4. LEFM of orthotropic materials

For an orthotropic material, the stress intensity factor of a sharp crack with a negligibly small FPZ may always be written in the form

$$K_{\mathrm{I}} = \sigma_N \sqrt{\pi D\alpha}\, F(\alpha) \quad (\alpha = a/D), \tag{24}$$

where σ_N = nominal stress, considered here at maximum load, D = characteristic dimension, a = crack length, α = relative crack length, and $F(\alpha)$ = function characterizing structure geometry and material orthotropy.

The energy release rate $\mathcal{G}$ may be related to K_{I} using Bao et al.'s (1992) generalization of Irwin's (1958) relation for orthotropic materials

$$\mathcal{G} = \frac{K_{\mathrm{I}}^2}{\bar{E}} = \frac{D}{\bar{E}} \sigma_N^2 g(\alpha), \quad g(\alpha) = \pi\alpha[F(\alpha)]^2, \tag{25}$$

where $g(\alpha)$ = dimensionless energy release function, characterizing the structure geometry and material orthotropy, and

$$\bar{E} = \frac{1}{Y(\rho)^2} \frac{(E_2/E_1)^{1/4}}{\sqrt{(1+\rho)/2E_1E_2}}, \quad \text{with } \rho = \frac{\sqrt{E_1E_2}}{2G_{12}} - \sqrt{\nu_{12}\nu_{21}}, \tag{26}$$

$$Y(\rho) = [1 + 0.1(\rho - 1) - 0.015(\rho - 1)^2 + 0.002(\rho - 1)^3][(\rho + 1)/2]^{-1/4}. \tag{27}$$

Subscripts 1 and 2 refer to Cartesian axes $x_1 \equiv x$ and $x_2 \equiv y$; x_2 coincides with the fiber direction; E_1, E_2, G_{12}, and ν_{12} are the orthotropic elastic constants; and parameters E_2/E_1 and ρ characterize the degree of orthotropy. The formula is valid when the crack propagates in the direction x_1 orthogonal to the fibers, but it is used here as an approximation even for propagation directions forming a small angle with x_1.

For fracture specimens in the form of long notched strip or slender notched beams, function $g(\alpha)$ or $F(\alpha)$ may be taken approximately the same as for isotropic specimens.

5. Asymptotic size and shape effect laws via equivalent LEFM

5.1. Case of long kink band or long notch

Following a procedure analogous to Bažant (1997), we will now try to express the coefficients of the size effect law (12) in terms of the energy release functions of LEFM. This will further allow us to capture the effect of structure geometry (shape). Assuming that the FPZ at the kink band front is not so large as to spoil linearity, the stress intensity factor K_{I} at the tip of a Mode I crack equivalent to the kink band may be expressed according to the principle of superposition as follows

$$K_{\mathrm{I}} = K_{\mathrm{I}}^P - K_{\mathrm{I}}^r, \tag{28}$$

in which

$$K_{\mathrm{I}}^P = \sigma_N \sqrt{D g(\alpha)}, \qquad K_{\mathrm{I}}^r = \sigma_r \sqrt{D \gamma(\alpha)} \qquad (\alpha = a/D). \tag{29}$$

Here a is the length of the equivalent LEFM crack, whose tip is expected to lie roughly in the middle of the FPZ; K_I^P or K_I^r are the LEFM stress intensity factors caused by load P acting alone (where P can represent not only one applied load but also the parameter of a system of loads), or by a uniform normal traction $\sigma = \sigma_r$ applied on the crack faces (but not the notch faces; Figure 5(a)); $g(\alpha)$ and $\gamma(\alpha)$ are dimensionless LEFM energy release functions of the orthotropic specimen.

When the kink band is propagating, $\mathcal{G} = G_b$ = fracture energy of the kink band. Its meaning, when a residual stress is present, is

$$G_b = J_{\mathrm{cr}} - \sigma_r \delta_r = \int_\delta \sigma \, d\delta_r - \sigma_r \delta_r = \int_\delta (\sigma - \sigma_r) \, \mathrm{d}\delta_r \tag{30}$$

Thus, in view of (25) and (28) with (29), we have $K_{\mathrm{I}}^P - K_{\mathrm{I}}^r = \sigma_N \sqrt{D g(\alpha)} - \sigma_r \sqrt{D \gamma(\alpha)} = \sqrt{\bar{E} G_b}$ ($= K_{\mathrm{I}b}$ = stress intensity factor of kink band). From this,

$$\sigma_N = \frac{\sqrt{\bar{E} G_b} + \sigma_r \sqrt{D \gamma(\alpha)}}{\sqrt{D g(\alpha)}}. \tag{31}$$

This formula, however, is not acceptable for small sizes of notched specimens; it yields $\sigma_N \to \infty$ for $D \to 0$ because $\lim g(\alpha) = g(\alpha_0) > 0$.

If there is no notch, a_0 represents the length of the portion of the kink band length along which the normal stress σ transmitted across the band has already been reduced to the residual

value σ_r. This is the distance from the notch mouth or from the beginning of the kink band to the beginning of the FPZ (Figure 5(a)).

By cutting geometrically similar notches of depth a_0 in specimens of suitable geometry with a suitable type of loading, one can achieve that the FPZ at maximum load be still attached to the notch tip. In that case, $\alpha_0 = a_0/D$ = constant for all the specimen sizes D, which is convenient for evaluating test data.

A basic question is what is the value of $a - a_0$ at the maximum load, $P_{\max}$. In view of extensive experimental evidence and finite element results for other quasibrittle materials (Bažant and Planas 1998), it is reasonable to introduce the following simplifying hypothesis: *The effective length $c_b = a - a_0$ of the FPZ of the kink band at $P_{\max}$ (Figure 5) is approximately constant, governed essentially by the microstructure.*

5.1.1. *Large-size asymptotics*

To deduce the large-size asymptotic behavior, we write $g(\alpha) = g(\alpha_0 + \theta)$ and $\gamma(\alpha) = \gamma(\alpha_0 + \theta)$ where

$$\theta = c_b/D, \quad \alpha = \alpha_0 + \theta \tag{32}$$

and expand functions g and γ into a Taylor series as powers of θ, centered at point α_0 (or $D \to \infty$). Then we truncate each series after the second (linear) term. So, we may introduce into (31) the large-size approximations

$$g(\alpha) \approx g_0 + g'\theta, \quad \gamma(\alpha) \approx \gamma_0 + \gamma'\theta, \tag{33}$$

in which $g_0 = g(\alpha_0)$, $\gamma_0 = \gamma(\alpha_0)$, and the primes denote the derivatives with respect to α; $g' = \mathrm{d}g(\alpha)/\mathrm{d}\alpha$, $\gamma' = \mathrm{d}\gamma(\alpha)/\mathrm{d}\alpha$ at $\alpha = \alpha_0$. With these approximations, one obtains the following size effect law for failures occurring only after a long stable kink band growth (Figure 8(a,b)))

$$\sigma_N = \frac{\sqrt{\bar{E}G_b} + \sigma_r\sqrt{\gamma' c_b + \gamma_0 D}}{\sqrt{g' c_b + g_0 D}}, \tag{34}$$

or, upon further algebraic rearrangement

$$\sigma_N = \frac{\sigma_0 + \sigma_Y\sqrt{1 + D/D_1}}{\sqrt{1 + D/D_0}}, \tag{35}$$

in which

$$D_0 = c_b\frac{g'}{g_0}, \qquad D_1 = c_b\frac{\gamma'}{\gamma_0}, \qquad \sigma_0 = \sqrt{\frac{\bar{E}G_b}{c_b g'}}, \qquad \sigma_Y = \sigma_r\sqrt{\frac{\gamma'}{g'}}. \tag{36}$$

Formula (35) has the following asymptotic values

$$\text{for large } D\text{:} \quad \sigma_N = \sigma_Y\sqrt{\frac{D_0}{D_1}} = \text{const.} = \sigma_r\frac{\gamma_0}{g_0}\sqrt{\frac{g'}{\gamma'}}, \tag{37}$$

$$\text{for small } D\text{:} \quad \sigma_N = \sigma_0 + \sigma_Y = \text{const.} \tag{38}$$

The size effect curve of $\log(\sigma_N - \sigma_Y)$ versus $\log D$ represents a smooth bridging between the size effect of plasticity (i.e. the case of no size effect, corresponding to a horizontal line) and the size effect of LEFM (i.e. the case of the strongest possible size effect, corresponding to a straight line of downward slope $-\frac{1}{2}$). The fact that the small-size asymptote is horizontal agrees with the fact that the strength theory or plasticity ought to be a good approximation for small sizes because the failure cannot localize.

Size D_0, called the transitional size, represents the intersection of the power scaling laws for plasticity and LEFM and characterizes the transition from plastic to brittle behavior. The ratio

$$\beta = D/D_0 \tag{39}$$

is a hypostatic characteristic called the brittleness number of a structure (Bažant and Planas 1998). For $\beta \to 0$, the structural behavior is perfectly ductile (plastic), and for $\beta \to \infty$ with $\sigma_R = 0$, the behavior is perfectly brittle, described by LEFM. Note that the shape effect on structural brittleness is included through function $g(\alpha)$ used to calculate D_0.

If the FPZ of the kink band is still attached to the tip at maximum load, $\gamma_0 = 0$ in (33), and so, for any structure geometry, the near-tip asymptotic behavior of function $\gamma(\alpha)$ for $\alpha \to \alpha_0$ is (see Appendix III)

$$\gamma(\alpha) = \gamma'\theta, \qquad \text{with } \gamma' = 8/\pi, \qquad \gamma' = \gamma'(\alpha - \alpha_0). \tag{40}$$

Thus (33) becomes a one-term linear approximation $\gamma(\alpha) \approx \gamma'\theta$ for $D \to 0$. This might not be sufficiently accurate for smaller D. For a broader range of sizes including small D, one must use at least a two-term approximation, $\gamma(\alpha) \approx \gamma'\theta + \frac{1}{2}\gamma''\theta^2$, or even better, not to replace $\gamma(\alpha)$ by an approximation. Thus, for notched specimens, the following formula should have a broader range of accuracy than (34)

$$\sigma_N = \frac{\sqrt{\bar{E}G_b} + \sigma_r\sqrt{D\gamma(\alpha)}}{\sqrt{g'c_b + g_0 D}} \quad \text{(FPZ at notch)}, \tag{41}$$

although it cannot be used if the structure is so small that $\alpha = \alpha_0 + c_b/D$ corresponds to a point that lies outside the structure or near its surface.

With the one-term linear approximation $\gamma(\alpha) = \gamma'\theta$, (31) and (34) reduce to the classical size effect law derived in 1984 for notched Mode-I (tensile) fracture specimens of positive geometry (i.e., those with $g' > 0$)

$$\sigma_N = \sqrt{\frac{\bar{E}G_B}{g'c_b + g_0 D}} = \frac{\sigma_0}{\sqrt{1 + D/D_0}} \quad \text{(FPZ at notch)}, \tag{42}$$

where

$$G_B = (K_b + \sigma_r\sqrt{\gamma' c_b})^2 / \bar{E} \quad \text{with } K_b = \sqrt{\bar{E}G_b}, \quad \gamma' = 8/\pi \tag{43}$$

Here K_b is the fracture toughness of the kink band, and G_B must be the same as in (15), representing the total fracture energy including the energy dissipation by σ_r. The value of γ' is independent of the structure geometry. Equation (42) is the special case of (35) for $D_1 \to \infty$.

Since functions $g(\alpha)$ and $\gamma(\alpha)$ capture the effect of structure geometry, the foregoing formulae give not only the effect of size but also the effect of shape.

5.1.2. *Small-size asymptotics*
To deduce the small-size asymptotic behavior, we introduce new parameter $\xi = 1/\theta = D/c_b$ and new LEFM functions

$$p(\alpha_0, \xi) = \xi g(\alpha_0 + \xi^{-1}), \qquad \omega(\alpha_0, \xi) = \xi \gamma(\alpha_0 + \xi^{-1}). \tag{44}$$

Then we substitute $g(\alpha) = p(\alpha_0, \xi)/\xi$ and $\gamma(\alpha) = \omega(\alpha_0, \xi)/\xi$ into (31), expand these functions into a Taylor series in ξ centered at point $\xi = 0$ (or $D \to 0$), and truncate the series after the second (linear) term, i.e.

$$p(\alpha_0, \xi) \approx p_0 + p'\xi, \qquad \omega(\alpha_0, \xi) \approx \omega_0 + \omega'\xi, \tag{45}$$

where $p_0, \omega_0, p', \omega' =$ constants. Expressing g and γ from (44) and substituting into (31), we obtain, after rearrangements,

$$\sigma_N = \frac{\sqrt{\bar{E}G_b} + \sigma_r\sqrt{\omega c_b + \omega' D}}{\sqrt{pc_b + p'D}}. \tag{46}$$

This expression can be brought to the form of the large-size asymptotic approximation (36) in which

$$D_0 = c_b\frac{p_0}{p'}, \qquad D_1 = c_b\frac{\omega_0}{\omega'}, \qquad \sigma_0 = \sqrt{\frac{\bar{E}G_b}{c_b p_0}}, \qquad \sigma_Y = \sigma_r\sqrt{\frac{\omega_0}{p_0}}. \tag{47}$$

5.1.3. *Asymptotic matching character*
For large enough sizes, the original formula (31) is more accurate than its subsequent approximations. But this formula is unacceptable for $D \to 0$, giving $\sigma_N \to \infty$. This conflicts with the small-size asymptotic form (46) which gives a finite σ_N. On the other hand, the approximations (35), (34), (41)and (42) of the large-size asymptotic formula happen to have also the correct small-size asymptotic behavior for $D \to 0$, approaching a horizontal asymptote. Moreover, they happen to have the same form as the small-size asymptotic approximation in (46). This means that these approximations serve as an interpolation between the opposite infinities (in the log D scale), generally called asymptotic matching.

There is a difference, though. In asymptotic matching, solutions that are accurate for one and the other infinity serve as the starting point. Here, however, the small-size approximation cannot be accurate in the limit for $D \to 0$ because it is based on LEFM while the FPZ is in the limit larger than the structure (properly one would need to use for the small-size limit the nonlocal theory of damage localization, which however does not seem amenable to a simple analytical solution). So the numerical values of $D_0, D_1, \sigma_0, \sigma_1$ for the small-size approximation cannot be reliably predicted. Therefore, the asymptotic matching with the small-size asymptotic approximation (46) can only indicate the form of the matched asymptotic formula but not its coefficients (in particular, the horizontal asymptote $\sigma = \sigma_0$ could be higher or lower than indicated by (47)). For this reason, we simply assume $D_0, D_1, \sigma_0, \sigma_1$ to be the same as

for the large-size asymptotic, and content ourselves with merely having the correct asymptotic form for $D \to 0$.

Since the justification of (35) rests in the matching of the asymptotic behaviors at opposite infinities, any smooth formula that satisfies the same small-size and large-size asymptotic properties should be equally valid; for instance,

$$\sigma_N = \frac{\sigma_0 + \sigma_Y[1 + (D/D_1)^r]^{1/2r}}{[1 + (D/D_0)^r]^{1/2r}}, \tag{48}$$

where r is any positive constant. This formula may be derived similarly as (35) except that one needs to set $\zeta = \theta^r$, $\tilde{g}(\alpha) = [g(\zeta)]^{1/r}$, $\tilde{\gamma}(\alpha) = [\gamma(\zeta)]^{1/r}$, and use instead of (33) the approximations $\tilde{g}(\zeta) = \tilde{g}_0 + \tilde{g}'\zeta$ and $\tilde{\gamma}(\zeta) = \tilde{\gamma}_0 + \tilde{\gamma}'\zeta$.

5.1.4. *Length of kink band at maximum load*

In the classical LEFM corresponding to $\sigma_r = 0$, specimens of positive geometry, i.e. those with $g'(\alpha_0) > 0$, attain $P_{\max}$ while the FPZ is still attached to the notch. Then a sufficient characteristic of $P_{\max}$ is that $\mathcal{G} = G_b$, which implies that the FPZ length $2c$ has grown to its full value $2c_b$. If the geometry is negative, $g'(\alpha_0) < 0$, the kink band propagates stably, at increasing load P, and $P_{\max}$ occurs at kink band length a such that $g'(\alpha) = 0$. When an R-curve, $R(c)$, is considered, the condition of $P_{\max}$ is that $\mathcal{G}'(a) = R'(c)$.

These conditions, however, do not apply if $\sigma_r > 0$. The total energy release rate due to P and σ_r may be written as $\mathcal{G} = K_{\mathrm{I}}^2/\bar{E}$ where $K_{\mathrm{I}} = [\sigma_N k(\alpha) - \sigma_r \kappa(\alpha)]\sqrt{D}$; $k(\alpha) = \sqrt{g(\alpha)}$ and $\kappa(\alpha) = \sqrt{\gamma(\alpha)}$ (dimensionless stress intensity factors of kink band). Under gravity load, the kink band is stable if $\mathcal{G}' > 0$ or $\mathrm{d}K_{\mathrm{I}}/\mathrm{d}\alpha > 0$, and it is critical (i.e., the load $P = P_{\max}$) if $\mathrm{d}K_{\mathrm{I}}/\mathrm{d}\alpha = 0$. This yields for gravity loading the conditions

$$k'(\alpha) < \kappa'(\alpha)\sigma_r/\sigma_N \text{..... stable, } P \text{ growing,} \tag{49}$$

$$= \text{ ..... critical, } P = \max. \tag{50}$$

The latter is of course the condition of maximum load for any type of loading (an equivalent equation without σ_N and in terms of $g(\alpha)$ was derived from the condition $\mathrm{d}\sigma_N/\mathrm{d}\alpha = 0$ by Zi, 1999).

If condition (50) is violated already while FPZ is attached to the notch tip ($\alpha_0 = \alpha_n$), $P_{\max}$ occurs right at the beginning of kink band propagation, i.e., as soon as $\mathcal{G} = G_b$. Otherwise the value of α_0 (location of the beginning of the FPZ at $P_{\max}$) along with $P_{\max}$ must be found by solving equations (42) and (50), in which $\alpha = \alpha_0 + c_b/D$ ($\approx$ coordinate of FPZ center).

Compared to propagation of cracks without residual stress, the range of stability of propagating kink bands is wider. According to (49), it includes not only negative but also positive values $g'(\alpha)$, up to a certain limit proportional to σ_r. So, a stable kink band growth can occur even for positive geometries (which is the case of the present tests). The previous difficulties in achieving stable pre-peak growth of a long kink band in experiments must have been due to unsuitable specimen and loading geometries (in post-peak, a stable growth further requires a sufficiently stiff loading).

5.1.5. *Other aspects*

Formula (12), which was derived for a long rectangular strip, is a special case of the general formula (35) for the case $D_1 = D_0$, i.e., for $\gamma(\alpha) = g(\alpha)$. The case of such an equivalence of the energy release functions means that the corresponding stress intensity factors are equal. This is immediately evident from the decomposition in Figure 10 based on the principle of superposition; indeed, the middle specimen is in a homogeneous stress state and thus has no stress singularity ($K_{\mathrm{I}} = 0$).

Formula (34) is of the same form as the formula derived in general for compression failures under the assumption that the laterally propagating damage band causing compression failure applies a uniform pressure on its boundaries (Bažant and Chen 1997, Eq. 51).

In a similar manner as shown in Bažant (1997) for cracked specimens, the foregoing analysis could be refined by considering that the kink band ought to exhibit R-curve behavior. In other words, the critical energy release may be expected to follow an R-curve, such that $\mathcal{G} = R_b(c)$ where $R_b(c)$ is assumed to be a given function of the kink band extension c. The only change needed in the preceding formulation is to replace the value $\sqrt{\bar{E}G_b}$ in (31) by $\sqrt{\bar{E}R_b(c)}$. In addition to this, it becomes possible to implement in the calculations the condition of failure as a stability limit, which can be reduced to the condition of tangency of the curve of energy release rate at constant load to the R-curve (Bažant 1997) (this condition cannot be imposed when the critical energy release rate is constant, being equal to G_b, as assumed in the preceding).

Similar to (14), Equation (35) is accurate only up to the first two terms of the power series expansion in $(1/D)$. Therefore, it could be generalized in the same manner as (16).

5.2. Case of kink band initiation from smooth surface

For kink bands originating from a smooth surface, one may usually assume that $P_{\max}$ occurs at the beginning of propagation, while the FPZ is still attached to the surface. Accordingly, the initial crack length for the LEFM approximation $a_0 = 0$ or $\alpha_0 = 0$. But the energy release rate of a crack of zero length vanishes, $g(\alpha_0) = \gamma(\alpha_0) = 0$. Thus, if we truncated the Taylor series expansion of $g(\alpha_0 + \theta)$ and $\gamma(\alpha_0 + \theta)$ after the linear term, we could not capture the size effect. Therefore we need to truncate these series only after the quadratic term. In this manner, the large-size approximation of (31) takes the form

$$\sigma_N = \frac{\sqrt{\bar{E}G_b} + \sigma_r\sqrt{\gamma' c_b + \gamma''(c_b^2/2D)}}{\sqrt{g' c_b + g''(c_b^2/2D)}} \quad \text{(FPZ at surface)}. \tag{51}$$

This may be rearranged as

$$\sigma_N = \frac{\sqrt{\bar{E}G_b/c_b} + \sigma_r\sqrt{\gamma'(1+2\chi_1)}}{\sqrt{g'(1-2\chi_0)}}, \quad \text{with } \chi_0 = -\frac{g'' c_b}{4g'D}, \quad \chi_1 = \frac{\gamma'' c_b}{4\gamma' D}, \tag{52}$$

with the notations $g' = \mathrm{d}g(\alpha)/\mathrm{d}\alpha$, $\gamma' = \mathrm{d}\gamma(\alpha)/\mathrm{d}\alpha$, $g'' = \mathrm{d}^2 g(\alpha)/\mathrm{d}\alpha^2$, $\gamma'' = \mathrm{d}^2\gamma(\alpha)/\mathrm{d}\alpha^2$, all evaluated at $\alpha = \alpha_0 = 0$; χ_0 is defined with a minus sign because g'' is negative in bending specimens (Bažant and Li 1996).

Equation (52), however, is not acceptable for small $D \to 0$ because it gives $\sigma_N \to 0$. Therefore, it is expedient to transform it by asymptotic approximations that do not change the

asymptotic behavior for $D \to \infty$ while making at the same time the formula acceptable for $D \to 0$. Such approximations are $\sqrt{1+2\chi_1} \approx (1+q\chi_1)^{1/q}$ and $1/\sqrt{1-2\chi_0} \approx (1+r\chi_0)^{1/r}$, with any positive constants r and q. For the case $r = q = 1$, after noting that $(1+\chi_1)(1+\chi_0) \approx 1+\chi_0+\chi_1$ for large D, we obtain a size effect formula identical to (22) (Figure 8(c)), in which

$$\sigma_\infty = \sqrt{\frac{\bar{E}G_b}{g'c_b}} + \sigma_r\sqrt{\frac{\gamma'}{g'}}, \tag{53}$$

$$D_b = -\frac{c_b}{4\sigma_\infty}\left[\frac{g''}{g'}\sqrt{\frac{\bar{E}G_b}{g'c_b}} + \sigma_r\left(\frac{g''}{g'} - \frac{\gamma''}{\gamma'}\right)\sqrt{\frac{\gamma'}{g'}}\right]. \tag{54}$$

A generalization in the form of (23) is also possible.

With (53), we have thus obtained a more general confirmation of (22). Note that although the approximations that led from (52) to (53) are only first-order accurate in $1/D$, (51) is first-order accurate in $1/D$ as well. So, these approximations cause no loss in accuracy overall. But (53) can be applied more widely because it has a realistic behavior also for $D \to 0$ while (52) does not.

5.3. Transition between long and short kink bands and universal size effect law

For small α_0, there must be a continuous transition between the size effect law for specimens with a notch or long kink band and that for specimens failing at kink band initiation from a smooth surface. A universal size effect law that describes this transition has already been developed for fracture of concrete ($\sigma_r = 0$; Bažant 1997). By a similar matching the asymptotic behaviors for long and short kink bands, a similar universal size effect law can be developed for kink bands.

6. Identification of fracture parameters from kink band tests

6.1. FPZ at notch tip

It is convenient to cut notches in the compression test specimens. The notch ensures the kink band to start in one place (which eliminates any possible statistical effect due to random spatial variation of local strength). Furthermore, if a suitable loading is used, it further ensures the FPZ at maximum load to be still attached to the notch tip. This brings about an important simplification—the value of α_0 can be controlled and thus is known.

The size effect formula for notched specimens, (14) with (43), can be used for identifying the fracture energy of the kink band, G_b, and the FPZ length, c_b, from the measurements of size effect. The procedure may be based on determining D_0 and σ_0 by fitting the formula (42) to maximum load data for notched specimens of sufficiently different sizes; then

$$c_b = D_0\frac{g_0}{g'}, \qquad G_B = \frac{c_b}{\bar{E}}g'\sigma_0^2. \tag{55}$$

If geometrically similar specimens and notches are used, α_0 = constant for all D. Geometrical similarity is not a requirement because the equivalent LEFM functions g and γ capture

the shape effect as well. Geometrical similarity, however, simplifies the evaluation of test results and improves the accuracy because the shape effect is known only approximately and thus introduces some additional error.

The fitting of (41) or (34) to σ_N data may be best accomplished the Levenberg–Marquardt nonlinear optimization algorithm. Alternatively, by algebraic rearrangement, equation (42) may be transformed to a linear regression plot $Y = AD + C$ for which

$$Y = \frac{1}{\sigma^2}, \qquad G_B = \frac{g_0}{A\bar{E}}, \qquad c_b = \frac{C}{A}\frac{g_0}{g'}. \tag{56}$$

The procedure is identical to that embodied in the RILEM Recommendation for concrete (whose statistical treatment and proper weighting is described in Bažant and Planas, 1998, Sec. 6.3).

According to (43), the kink band fracture energy may then be calculated as

$$G_b = (\sqrt{\bar{E}G_B} - \sigma_r\sqrt{\gamma' c_b}) / \bar{E}, \tag{57}$$

provided that σ_r is determined separately.

An approximate way to estimate σ_r may be to measure the residual load on very large specimens, provided that a post-peak plateau can be reached. Additional damage long after the peak load, however, may further reduce the stress in the kink band, making it hard to identify a plateau. An upper bound on σ_r is provided by the compression strength of very small specimens with nearly uniform stress distribution at peak load.

Another way to determine σ_r may be to test both notched and unnotched specimens, and use the Marquardt–Levenberg optimization algorithm to fit the maximum load data by (41) and (51), considering G_b, c_b and σ_r as three unknowns.

Still another way to determine σ_r might be to measure under uniaxial compression the post-peak behavior of very small unnotched prismatic specimens – so small that the FPZ of the kink band would occupy the whole cross section, thus ensuring simultaneous (nonpropagating) failure.

It is instructive to relate G_B to the J-integral. Consider the J-integral path starting at point C in Figure 11 (top) of the imagined cohesive crack representing the kink band. Point C lies immediately ahead of the tip of the notch, and so the J integral along the path starting at C represents the total energy flux into the cohesive crack equivalent to the kink band. When the extension of this crack (or kink band) is sufficient to reduce the stress at point C to the residual stress σ_r, the full fracture energy G_b of the kink band comes into play, and then, by a similar derivation as that which led to (10), the J-integral along the path starting at C, which must be equal to G_B, is $J_{cr} = G_B$, $G_B = G_b + \sigma_r\delta_r$ (Equation 10) where δ_r is the normal displacement (contraction) across the kink band at the notch tip (or the end of the FPZ), and G_b is the fracture energy representing the cross-hatched triangular area in Figure 7 (bottom). Knowing σ_r, this relation can be used to estimate the value of δ_r.

The value of δ_r ought to be equal to the opening displacement of the equivalent LEFM crack at the location of the notch tip (Figure 11). This displacement may be calculated from the parabolic asymptotic profile of the equivalent LEFM crack, whose tip lies at distance c_B from the notch tip. According to the well-known formula (e.g. Eq. 5.5.11 in Bažant and Planas 1998), one may use the approximation

$$\delta_r = \sqrt{32G_B c_b/\pi\bar{E}}. \tag{58}$$

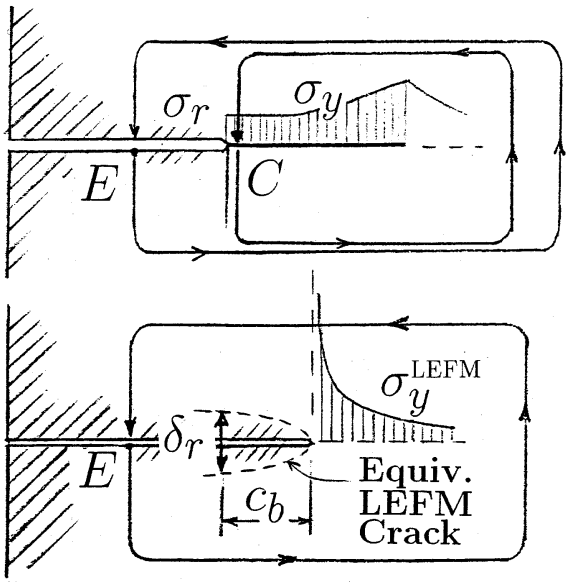

Figure 11. Equivalent cohesive crack emanating from the notch tip (top), equivalent LEFM crack (bottom), and J-integral paths.

6.2. FPZ REMOTE FROM NOTCH AND SPECIMENS WITH END RESTRAINT

While the rotational restraint at the ends of the present carbon-PEEK specimens has made it possible to demonstrate a long stable growth of kink band, it has slightly complicated the analysis of test results. The restraint causes the axial load resultant P to gradually shift to the right in Figure 1(a) as the kink band propagates, i.e., the resultant eccentricity e (Figure 1(a) and 13) increases as a function of α. Function $e = e(\alpha)$ is determined by the condition that the relative rotation between the specimen ends $\phi = PC_{PM} + MC_{MM} + \sigma_r C_{Mr} = 0$ where $M = Pe$ = moment of the resultant. Consequently,

$$e(\alpha) = \frac{-[PC_{PM}(\alpha) + \sigma_r C_{Mr}(\alpha)]}{PC_{MM}(\alpha)} \quad (P = \sigma_N bD). \tag{59}$$

The compliances, according to well-known LEFM relations (e.g. Bažant and Planas 1998, Eq. 3.5.18), are

$$C_{PM}(\alpha) = \frac{2}{b\bar{E}} \int_0^\alpha k_P(\alpha') k_M(\alpha')\, \mathrm{d}\alpha', \qquad C_{MM}(\alpha) = \frac{12\,L}{bD^3\bar{E}} + \frac{2}{b\bar{E}} \int_0^\alpha [k_M(\alpha')]^2\, \mathrm{d}\alpha',$$

$$C_{Mr}(\alpha) = \frac{2}{b\bar{E}} \int_0^\alpha k_M(\alpha') k_r(\alpha')\, \mathrm{d}\alpha', \tag{60}$$

where b, L = specimen thickness and length (Figure 1(a)), and the k's are the dimensionless stress intensity factors for unit loading by P, M or σ_r; $k_P = K_{\mathrm{I}}^P b\sqrt{D}/P$, $k_M = K_{\mathrm{I}}^M bD^{3/2}/M$ and $k_r = K_{\mathrm{I}}^r/\sigma_r\sqrt{D}$. Also,

$$g(\alpha) = \sigma_N^2 D\{k_P(\alpha) + k_M(\alpha)e(\alpha)/D\}^2. \tag{61}$$

According to Tada et al. (1985), $k_P(\alpha) = \sqrt{\pi\alpha}(1.122 - 0.231\alpha + 10.55\alpha^2 - 21.71\alpha^3 + 30.38\alpha^4)$, $k_M(\alpha) = \sqrt{\pi\alpha}(1.122 - 1.40\alpha + 7.33\alpha^2 - 13.08\alpha^3 + 14.0\alpha^4)$. For k_r see Appendix IV.

If σ_r were 0, then the failure after a long kink band growth, observed in the present carbon-PEEK tests, would have to be characterized by $g'(\alpha) = 0$, which would require the use of formulae based approximating $g(\alpha + c_b/D)$ up to the quadratic term in c_b/D. However, because σ_r is not 0 (nor negligible), the formulae based on approximation up to the linear term are appropriate.

To identify the values of G_b, c_b, α_0 and σ_r from the present carbon-PEEK tests, equation (59) and the expression $\alpha = \alpha_0 + c_b/D$ must first be substituted into (42) and (50). Then the standard library subroutine for the Levenberg–Marquardt nonlinear optimization algorithm may be used to minimize the sum of the squares of (50) and of the deviations of (42) from the data points.

To succeed, the tests must cover a sufficient range of brittleness number $\beta = D/D_0$. If the range of β is too limited, the fitting problem may be ill-conditioned. Then one needs to drop σ_r from the set of unknown variables in the least-square fitting, and estimate σ_r in advance by other means, as already discussed (e.g., from measurements of post-peak behavior), or use in data fitting various estimated fixed values of σ_r and then compare the results.

In the present study, however, the values of e and α_0 at $P_{\max}$ have not been calculated by the aforementioned procedure. Rather, for the sake of simplicity, the values that were already available from a finite element simulation with the cohesive crack model carried out earlier by G. Zi have been used in fitting (42) to the data points in Figure 12 (top left). This furnished the following material parameters of the carbon-PEEK composite tested

$$G_b = 27.9\,\text{kN/m}, \qquad c_b = 0.70\,\text{mm}, \qquad \sigma_r/\sigma_0 = 0.436, \qquad \sigma_0 = 758\,\text{MPa}. \tag{62}$$

Figure 12 on top right shows also a comparison of the data with the size effect plot based on the material parameters obtained with the cohesive crack model. The plot is very close to that in Figure 12 on top left.

It is instructive to compare these values to those obtained by simple fitting of the data with the size effect law (14) shown in Figure 13. They are $\sigma_0 = 779\,\text{MPa}$ and $c_b = 18.5\,\text{mm}$. Although σ_0 is about the same, c_b is far too large, by an order of magnitude. This demonstrates that the differences in e/D and α_0 among specimens of different sizes cannot be neglected.

6.3. Test simulation by cohesive crack model

Simulations of the present and other tests with the cohesive crack model will be reported separately (Bažant and Zi, 1999). Two-dimensional elastic finite element analysis has been applied to obtain the compliance matrices for forces and displacements at the specimen ends and at the nodal points placed on the sides of the kink band. The condition that the kink band contraction indicated by the softening stress-displacement law must be compatible with the elastic deformation of the specimen leads to one integral equation, and the condition that the stress intensity factor at the kink band front must vanish leads to another. Based on the nodal point discretization, both integral equations are approximated by a system of algebraic equations, which is then solved by incremental loading.

A computer program for calculating the values of $P_{\max}$, $e(\alpha)$ and α_0 from any given values of G_b, c_b and σ_r has been written. The values of G_b, c_b and σ_r have then been optimized so

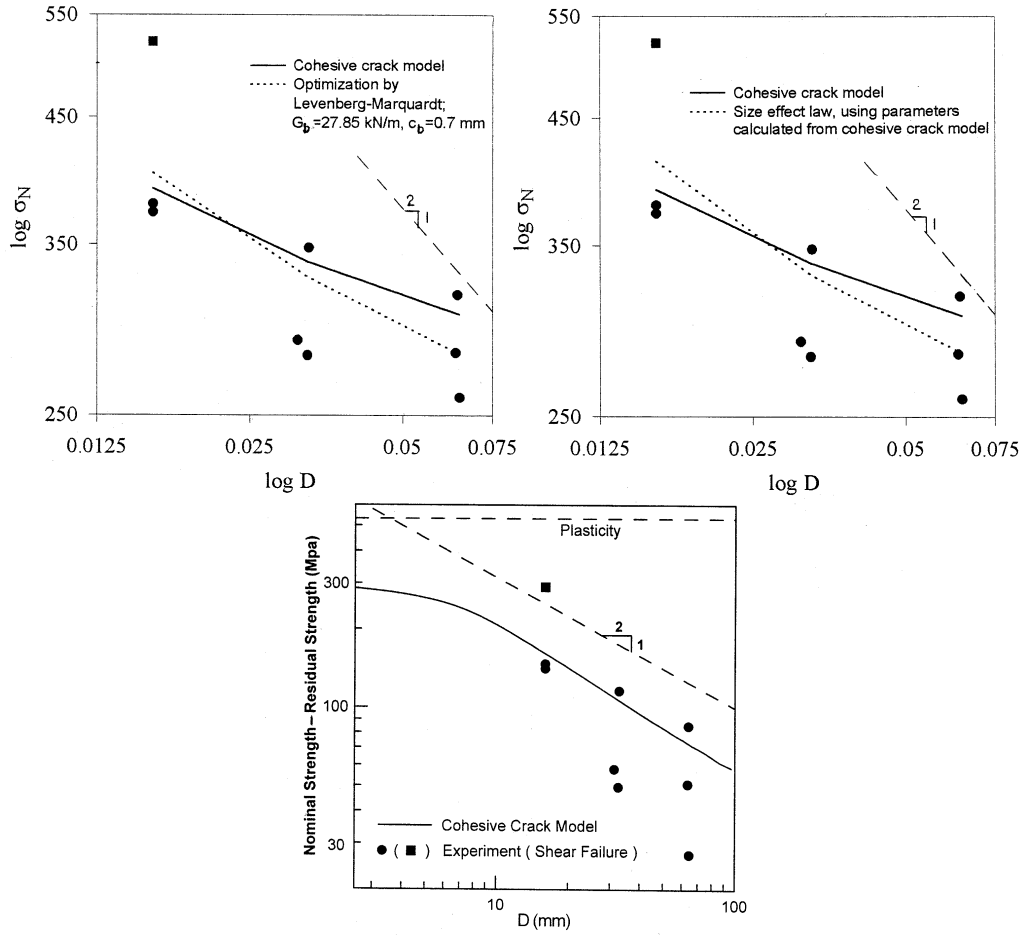

Figure 12. Optimum fits by size effect formulae and by numerical analysis with the cohesive crack model.

as to obtain the best possible fit of the test data. In the process, eccentricities e have also been determined.

The calculated subsequent stress profiles throughout the ligament, along with the corresponding eccentricities e of the load resultant, are shown in Figure 14. The optimum fit of the test data by the cohesive crack model, with $\log(\sigma_N - \sigma_r)$ as the ordinate, is shown by the curve in Figure 12 (bottom). The corresponding optimum value of fracture energy is $G_b = 28.2\,\text{kN/m}$, which is almost the same as in (62), but the length of the softening segment (Figure 14), which is about 2.7 mm for all D, is almost twice as large as $2c_b$. This suggests that the tip of the equivalent LEFM crack might not be at the center of the FPZ but farther behind its front. The optimum fit, however, is not very sensitive to c_b; this is documented by Figure 12 (top left and right), with $\log \sigma_N$ as the ordinate, which shows the optimum fit by the cohesive crack model (solid curve) and the results from (42) based on the optimum material parameters obtained with the cohesive crack model. Note that the dashed curves in Figure 12 on top left and right, corresponding to rather different c_b, are not very different. To eliminate this ambiguity, tests of a broader size range or fitting of post-peak response would be needed.

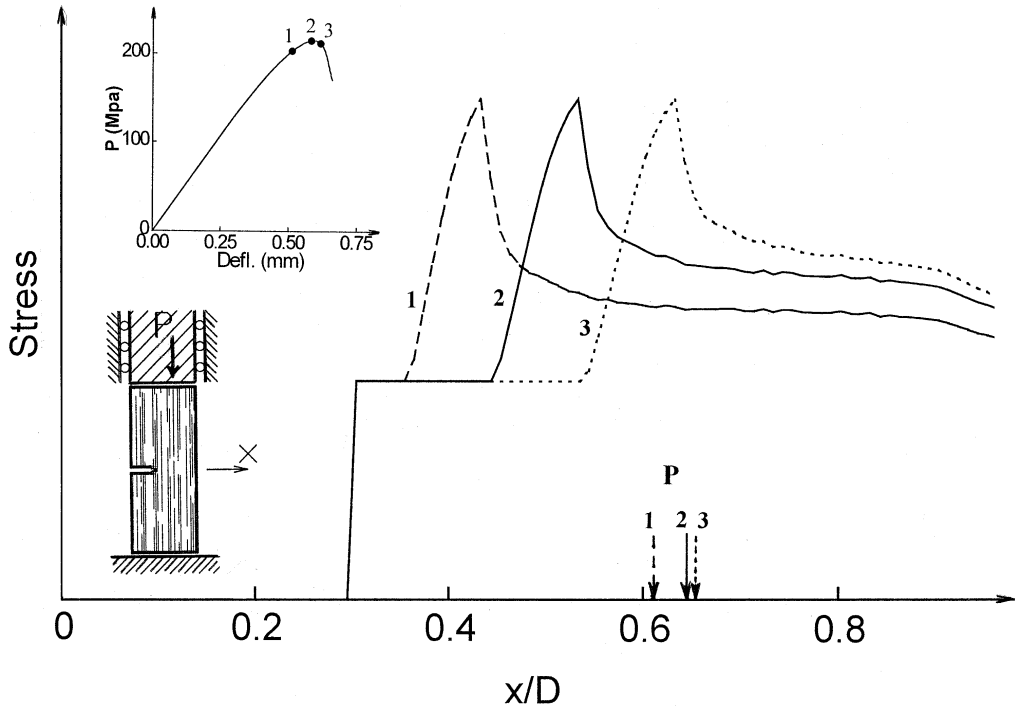

Figure 13. Stress profiles across the ligament of the carbon-PEEK specimens before, at and after the maximum load (note the shift of the compression resultant P which makes a stable kink band growth possible).

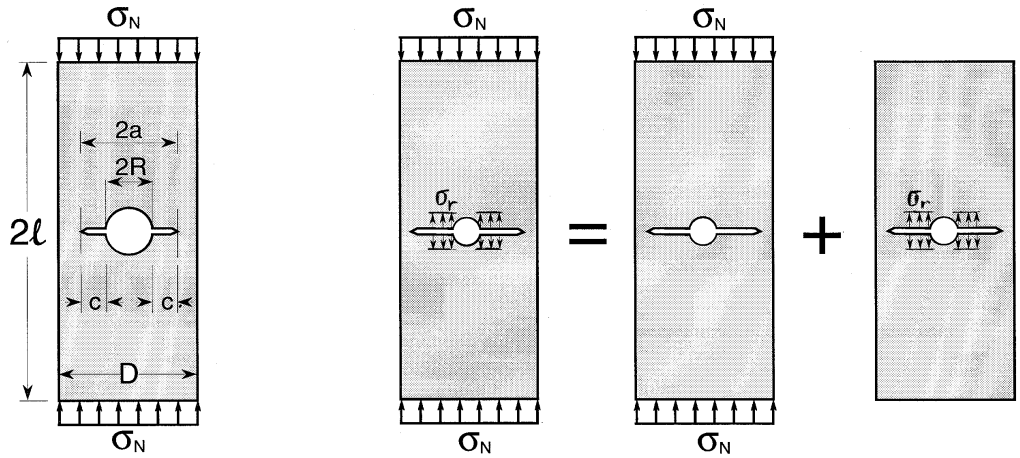

Figure 14. Constant-size carbon-epoxy specimen with holes of various diameters used by Soutis, Curtis and Fleck (1993).

7. Soutis et al.'s tests of carbon-epoxy laminates with holes of various sizes

The studies of kink band failures of composites have so far not been focused on the size effect. No data for geometrically similar specimens seem to be available in the literature. However, since functions $g(\alpha)$ and $\gamma(\alpha)$ characterize the shape effect, test data on nonsimilar specimens exhibiting the effect of shape can also be used to check and calibrate the theory provided that the range of the brittleness number $\beta = D/D_0$ in (12) is sufficient. The recent test data of

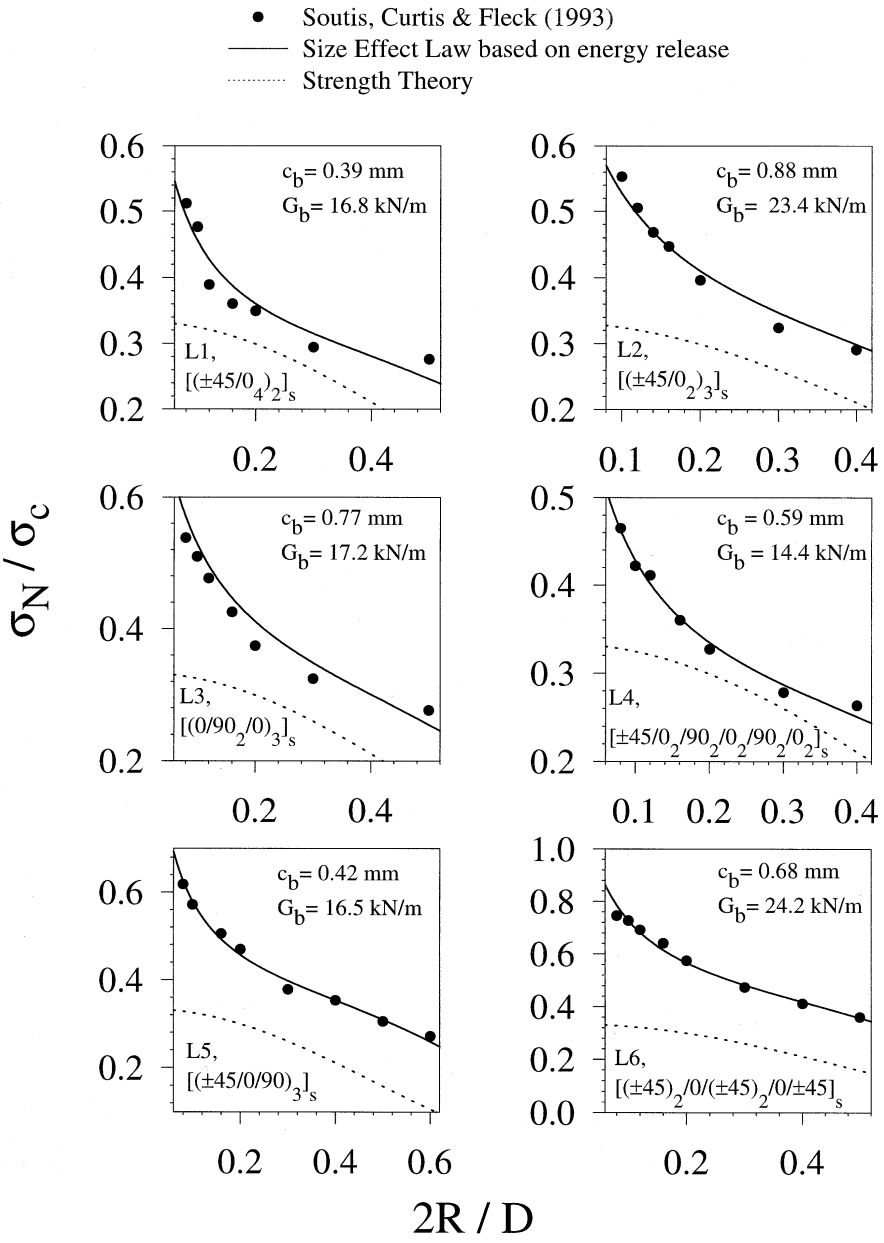

Figure 15. Soutis, Curtis and Fleck's (1993) test results for quasi-isotropic and orthotropic carbon–epoxy laminates of six different layups, with holes of various radii R (data points) and constant width D. Solid curves: optimum fits by size-shape effect law in (31). Dashed curves: predictions of strength theory exhibiting no size effect.

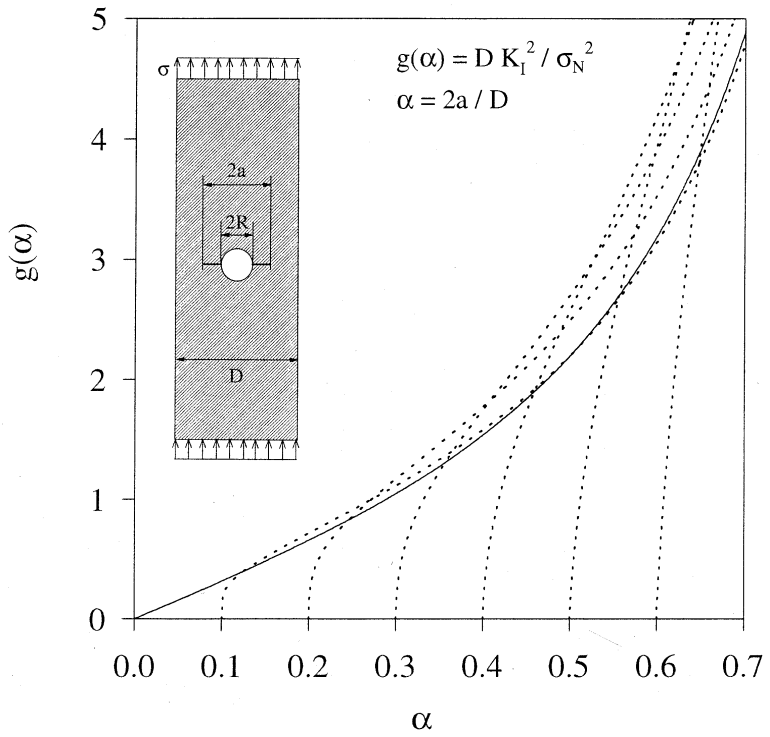

Figure 16. Dimensionless energy release function $g(\alpha)$ for isotropic specimens with centric holes of different radii (derived by Führing, 1973).

Soutis and Fleck (1991), Soutis, Fleck and Smith (1991), and Soutis, Curtis and Fleck (1993) exhibit a broad enough range of brittleness numbers, attained not through a variation of the overall specimen size D (which was kept constant) but through a variation of D_0.

Soutis et al. (1991) used rectangular panels of constant width D to study how centric holes of various radii R affect the compressive strength of unidirectional and multidirectional carbon/epoxy (T800/924C) laminates of different layups, labeled as L1 to L6 (Figure 14 left). The specimens were 50 mm wide, 245 mm long and 3 mm thick, and the diameter–width ratio $2R/D$ varied from 0.08 to 0.60 for each layup. The results, shown by the data points in Figure 15, offer another possibility to check the present theory for a different geometry and a different material, and to compare it to the classical strength theory.

The layups of laminates of Soutis et al. were either quasi-isotropic of only weakly orthotropic. Thus the corrections for orthotropy are either unnecessary or almost unimportant for these tests. In view of the fact that, for long cracked strips without holes, the same dimensionless energy release functions can be used as for isotropic specimens (Bao et al. 1992), it is assumed that the same can be done for specimens with holes, at least as an approximation.

Therefore, the effect of the mild orthotropy of some of the Soutis et al.'s laminate layups is taken into account only through $\bar{E}$. With this assumption, the analysis of these data is made easy by the availability of the solution of the stress intensity factor K_{I} (Führing 1973, and Murakami's 1987 handbook, p. 291) for an in finite strip with a hole, which may be used as an approximation for a rectangular specimen with a hole (Figure 14). This solution, used here for compressive instead of tensile loading, is shown in Figure 16 where $\alpha = (c + R)/D$. As seen, the curve of K_{I} as a function of α first quickly rises as the horizontal cracks grow from

the sides of the hole (Figure 14 left and Figure 16 insert). But soon the slope diminishes as this curve approximately joins the solid curve in Figure 16, which corresponds to $K_I(\alpha)$ for a specimen containing a centric horizontal crack (of relative depth α) instead of a hole.

By virtue of similarity transformations, the slope of the initial rise of the curve must be the same as for a crack starting from the surface of an elastic halfspace. For such a crack, $K_I = 1.12\sigma\sqrt{\pi c}$, which implies that $g(\alpha) = K_I^2/\sigma^2 D = 1.12^2\pi c/D$ and $g'(\alpha) = 1.12^2\pi < \infty$. The formula plotted in Figure 16, however, gives an infinite (vertical) initial slope, which means that its initial portion cannot be accurate. Because of this asymptotic inaccuracy, g' (at $c = 0$) in (51) for cracks initiating from a smooth surface is obtained, incorrectly, as infinite, which precludes using this equation and forces us to use the original equation (31) from which (51) was derived. Nevertheless we assume that for the present finite values of c the formula plotted in Figure 16 is accurate enough.

The maximum load may be expected to be reached only after the slope of the curve in Figure 16 diminishes and the solid curve is approached, which means that the specimen behaves roughly as a panel with a large centric crack of length $2(R + c)$. This is another reason why the general original formula (31), rather than formula (51) derived from it for a kink band initiating from a smooth surface, appears to be appropriate.

Let us now assume the FPZ of the kink band at maximum load is still attached to the hole. In that case, the equivalent LEFM crack should have its tip roughly at the distance $c = c_b$ from the hole. This value of c is large enough for approaching the solid curve in Figure 16, i.e., a lies in Figure 16 beyond the sharp decrease of slope of the curves. But then the truncation of the series expansion after the second term that was made in deriving (12) would not be accurate enough. Therefore, the original formula (31) is used.

In (31), we now have $\alpha = 2(R + c)/D \approx 2(R + c_b)/D$. Functions $g(\alpha)$ and $\gamma(\alpha)$ are the dimensionless energy release functions corresponding to the case of a tensioned cracked plate with a centric hole and a pair of cracks, loaded either at the specimen ends or along a portion of each crack (Figure 14 right); see the Appendix. The value of the residual stress σ_r needs to be considered as 0 because the FPZ of the kink band is still attached to the hole when the maximum load is reached. Considering G_b and c_b as unknowns, Equation (31) has been fit to the data of Soutis et al. (1993) using the Levenberg-Marquardt nonlinear optimization algorithm. The results, shown by the solid curves in Figure 15, are quite satisfactory. The optimum values of G_b and c_b corresponding to these fits are indicated in each plot in Figure 15 (and $\sigma_r = 0$).

To check whether a theory capable of representing the size effect is necessary, the test results are further compared to the simplest version of a theory that exhibits no size effect – the strength theory in which it is assumed that the specimen fails as soon as the vertical normal stress at the sides of the hole reaches the strength of the material. The dashed curves in Figure 15 show the predictions of the strength theory (obtained under the assumption that the material strength is the same as used in the kink band analysis). Obviously the trend of those curves does not agree with the trend of the data. These comparisons provide additional support for the present theory. They reveal that a theory exhibiting the size effect is necessary to describe Soutis et al.'s test results well.

The reason that the last data points on the right of the plots for specimens L1, L3 and L4 in Figure 15 systematically deviate slightly upwards from the solid curves for the present theory could be that (31) is not acceptable for large holes (because the cracks at maximum load are not long enough for approaching the solid curve in Figure 16).

8. Conclusions

(1) Transverse slanting of the notch in test specimens of carbon-PEEK laminate can achieve pure out-of-plane kink band failure, not contaminated by shear splitting cracks.

(2) Restraining specimen ends against rotation helps to stabilize kink band growth and makes it possible to demonstrate the possibility of a stable growth of long kink bands before the peak load.

(3) Compression tests of notched carbon-PEEK specimens show that the nominal strength of geometrically similar notched specimens failing purely by kink band propagation exhibits a strong (non-statistical) size effect.

(4) The size effect observed is transitional between the asymptotic case of no size effect, which is characteristic of plasticity or any theory whose failure criterion is expressed solely in terms of stress or strain, and the asymptotic case of size effect of linear elastic fracture mechanics, which is governed by energy release.

(5) The results of the present carbon-PEEK tests roughly agree with the approximate general size effect law proposed by Bažant (1983, 1984) and derived recently by asymptotic analysis of energy release (Bažant 1997).

(6) The present theory gives not only the effect of size but also the effect of shape. The theory is found to agree with the recent shape effect tests of Soutis et al. (1993), which utilized constant-size carbon epoxy specimens with centric holes of different diameters.

(7) The nominal strength of specimens failing at the initiation of a kink band from a smooth surface is also predicted to exhibit a size effect. A simple size effect formula is derived for this case, too. This formula is the same as that previously derived for the size effect on the modulus of rupture measured in bending tests of notch-free specimens.

(8) In addition to previous derivations, the size effect law for specimens with notch of long kink band can also be derived by J-integral analysis of energy release, as well as from the recently proposed nonlocal LEFM.

(9) The size effect law for notched specimens permits the fracture energy of the kink band and the length of the fracture process zone at the front of the band to be easily identified solely from the measurements of maximum loads.

(10) The results suggest that the current design practice, in which the compression failure is predicted on the basis of strength criteria (or plasticity), thus inevitably missing the size effect, is acceptable only for small specimens or structural parts. In the interest of safety, it should be revised for large structural parts.

Remark on statistical size effect. According to the arguments in Bažant and Planas (1991, ch. 12), this size effect, not addressed here, is overpowered by the present energetic size effect. It is significant only for

(1) very small notched specimens for which the FPZ involves most of the cross section;
(2) unnotched specimens so large that the energetic size effect approaches its horizontal asymptote (Figure 8(c)), and
(3) uniformly stressed specimens with negligible FPZ reaching peak load at fracture inititiation (probably relevant to Kyriakides and Ruff, 1997).

Appendices

I. K_I FOR ISOTROPIC PANEL WITH HOLE AND CRACKS

The stress intensity factor for an isotropic panel with a circular hole and two cracks (Figure 14 and 16) may be written as $K_I = \sigma\sqrt{D}k(\alpha)$ (e.g. Bažant and Planas, 1998, Sec. 5.1) where $k(\alpha)$ = function of α. Then $g(\alpha) = k^2(\alpha)$. The solution of K_I for a cracked rectangular panel with a centric hole (Figure 14 and 16 insert) was obtained by Führing (1973) (see also Murakami, 1987, p. 291). With the notations $\alpha = a/D$, $\bar{\alpha} = \pi\alpha$, $\delta = b/R$, $\gamma = 2R/D$, $\beta = (2\alpha - \gamma)(1 - \gamma)$, one gets $g(\alpha) = 2\pi\alpha F^2(\alpha)$ where $F(\alpha) = \phi\psi$ and

$$\phi = \frac{1}{\pi - 1}\left\{\pi\sqrt{\frac{1}{\bar{\alpha}}\tan\bar{\alpha} + g\sin(2\bar{\alpha})}\left(1 + \frac{\epsilon^2(2-\epsilon^2)}{1-\varepsilon}\right) + \sqrt{1+2g}\right\}, \tag{63}$$

$$\psi = \xi\left(3\beta^{2P/3} - 2\beta^P\sqrt{\xi}\right). \tag{64}$$

Here $g = 0.13\left[(2/\pi)\arctan\delta\right]^2$, $\epsilon = (\alpha/\pi)\arctan(0.6\sqrt[3]{\delta})$, $P = \log(\xi^{-3/2})/\log(\beta^*)$, $\beta^* = \gamma\delta/[\gamma(2\delta - 1) + 1]$ and $\xi = 1 + (2/\pi)\arctan(1.5\sqrt{\delta})$.

II. K_I FOR ISOTROPIC PANEL WITH A HOLE LOADED ON A PORTION OF CRACK LENGTH

The stress intensity factor for an isotropic panel in which the crack lips are subjected to a distributed load of resultant P in each crack was calculated by Newman (1982). With the notations R = radius of the hole, a = crack length, $\alpha = a/D$, $\lambda = R/a$, $\beta_1 = b_1/a$, $\beta_2 = b_2/a$, b_1 or b_2 = distance between the initial or terminal points of the loaded crack segment (Figure 14 right), respectively,

$$\gamma(\alpha) = (8/\pi)\alpha(\arcsin\beta_2 - \arcsin\beta_1)F_3F_4, \tag{65}$$

where

$$F_3 = \frac{G(\beta,\lambda)}{\arcsin\beta_2 - \arcsin\beta_1}, \qquad F_4 = \frac{\arcsin B_2 - \arcsin B_1}{\arcsin\beta_2 - \arcsin\beta_1}\sqrt{\sec\pi\alpha}, \tag{66}$$

$$G(\beta,\lambda) = \left[\left(1 + \frac{A_1}{1-\lambda} + \frac{3A_2}{2(1-\lambda)^2}\right)\arcsin\beta + \left(\frac{A_1}{1-\lambda} + \frac{(4-\beta)A_2}{2(1-\lambda)^2}\right)\sqrt{1-\beta^2}\right]_{\beta_1}^{\beta_2}, \tag{67}$$

with $A_1 = -0.02\lambda^2 + 0.558\lambda^4$ and $A_2 = 0.221\lambda^2 + 0.046\lambda^4$, and $B_1 = \sin(\pi b_1/D)\ /\ \sin\pi\alpha$, $B_2 = \sin(\pi b_2/D)\ /\ \sin\pi\alpha$.

III. PROOF OF EQUATION (40)

Equation (40) is proven by noting that the stress intensity factor K_I caused by σ_r when $c = c_b \ll a_0$ is the same as for a crack of length $2a$ in an infinite body, loaded on the crack faces

by σ_r over distance $c_b \ll a$ from one tip. By superposition of a well known formula (e.g. Tada et al., 1985) used to derive Dugdale model

$$K_{\mathrm{I}} = \int_{a-c}^{a} k_P(x)(\sigma_r \mathrm{d}x) \approx \sigma_r \sqrt{\frac{8c}{\pi}}, \qquad k_P(x) = \frac{1}{\sqrt{\pi a}} \sqrt{\frac{a+x}{a-x}} \approx \sqrt{\frac{2}{\pi(a-x)}}, \tag{68}$$

where $k_P(x)$ = Green's function for the effect on K_{I} of a concentrated crack-face load pair at distance x from the crack center. Then $\gamma = K_{\mathrm{I}}^2/\sigma_r^2 D \approx (8/\pi)c/D$.

IV. Stress intensity factor due to σ_r

By superposition of the solution for crack-face concentrated load pair in infinite edge-cracked strip (Tada et al., 1985)

$$k_r(\alpha) = \int_{\alpha_{\mathrm{notch}}}^{\alpha} (1-\alpha)^{-3/2} (1 - t^2/\alpha^2)^{-1/2} \sum_{n=1}^{4} g_n(\alpha)(t/\alpha)^{n-1} \mathrm{d}t, \tag{69}$$

$$\begin{aligned}
g_1(\alpha) &= 0.46 + 3.06\alpha + 0.84(1-\alpha)^5 + 0.66\alpha^2(1-\alpha)^2, \\
g_2(\alpha) &= -3.52\alpha^2, \\
g_3(\alpha) &= 6.17 - 28.22\alpha + 34.54\alpha^2 - 14.39\alpha^3 - (1-\alpha)^{3/2} \\
&\quad -5.88(1-\alpha)^5 - 2.64\alpha^2(1-\alpha)^2, \\
g_4(\alpha) &= -6.63 + 25.16\alpha - 31.04\alpha^2 + 14.41\alpha^3 + 2(1-\alpha)^{3/2} \\
&\quad +5.04(1-\alpha)^5 + 1.98\alpha^2(1-\alpha)^2.
\end{aligned}$$

V. Comment on application of nonlocal LEFM

All the size effect equations presented here, along with their large-size and small-size asymptotic forms, can alternatively be derived from nonlocal fracture mechanics – a new general model (Bažant 1998b) proposed as a simpler alternative to the cohesive crack model and equivalent to it asymptotically for large sizes. This model is based on the smeared-tip superposition method (Bažant and Planas 1998, Sec. 7.5.6) in which the stress tensor $\boldsymbol{\sigma}(\boldsymbol{x}, a)$ and displacement vector $\boldsymbol{v}(\boldsymbol{x}, a)$ at any point of coordinate vector $\boldsymbol{x}$ in a body with the FPZ centered at crack length a (kink band length) is represented as a superposition of LEFM solutions for crack (kink band) tips within the FPZ corresponding to loads $Pq(\zeta)\mathrm{d}\zeta$, i.e.

$$\begin{aligned}
\boldsymbol{\sigma}(\boldsymbol{x}, a) &= \sigma_N \int_{-1}^{1} \boldsymbol{S}(\boldsymbol{\xi}, \alpha + \zeta c/D)\, q(\zeta)\, \mathrm{d}\zeta, \\
\boldsymbol{v}(\boldsymbol{x}, a) &= \sigma_N \frac{D}{\bar{E}} \int_{-1}^{1} \boldsymbol{V}(\boldsymbol{\xi}, \alpha + \zeta c/D)\, q(\zeta)\, \mathrm{d}\zeta.
\end{aligned} \tag{70}$$

Here $\alpha D = a$ = length of crack equivalent to kink band at FPZ center, $\alpha D + \zeta c$ = crack (kink band) lengths at various points along the FPZ; the crack (kink band) lengths in FPZ

occupy the interval $(a - c, a + c)$ corresponding to $\zeta \in (-1, 1)$; $q(\zeta)$ = dimensionless load distribution function such that $\int_{-1}^{1} q(\zeta)\,\mathrm{d}\zeta = 1$. The dimensionless functions $\boldsymbol{S}(\boldsymbol{\xi}, \alpha')$ and $\boldsymbol{V}(\boldsymbol{x}, \alpha')$ represent the stress tensor and displacement vector at relative coordinate vector $\boldsymbol{\xi} = \boldsymbol{x}/D$ in a body with crack (kink band) length $a' = \alpha' D$, calculated by LEFM for $\sigma_N = 1$ (or for load $P = bD$). The half-length, c, of FPZ is taken as the smaller of c_b and the distance from FPZ center to the notch tip or the surface of the body. In the smeared-tip method, the stresses and displacements on the crack line expressed from (70) are substituted into the stress-separation function of the cohesive crack model, which yields a singular integral equation for $q(\zeta)$. To solve the size effect from that equation is not easy. Therefore it was proposed to avoid prescribing a functional relation between the crack-bridging stress and the crack opening (separation), and introduce instead the *hypothesis* that the FPZ propagation is decided by the average of $g(\alpha)$ over the FPZ, i.e., by the condition

$$\frac{\sigma_N^2}{E}\, D\, \overline{g}(\alpha) = G_b, \qquad \text{with } \overline{g}(\alpha) = \int_{-1}^{1} g(\alpha + \zeta c/D)\, q(\zeta)\,\mathrm{d}\zeta. \tag{71}$$

Acknowledgment

Grateful acknowledgment is due to the Office of Naval Research (monitor Yapa D.S. Rajapakse) for partial financial support under grants N00014-91-J-1109 (directed by Bažant) N00014-96-1-1219 (directed by Daniel) to Northwestern University. J.-J.H. Kim, E. Becq-Giraudon and M. Brocca wish to thank ONR for financial support under the former grant.

References

Argon, A.S. (1972). Fracture of composites. *Treatise of Materials Science and Technology*, vol. 1, p. 79, Academic Press, New York.

Bao, G., Ho, S., Suo, Z. and Fan, B. (1992). The role of material orthotropy in fracture specimens for composites. *International Journal of Solid Structures*, **29**(9), 1105–1116.

Bažant, Z.P. (1976). Instability, ductility, and size effect in strain-softening concrete. *Journal of Engineering Mechanics Division*, Am. Soc. Civil Engrs., **102**, EM2, 331–344; disc. **103**, 357–358, 775–777, **104**, 501–502.

Bažant, Z.P. (1983). Fracture in concrete and reinforced concrete, Preprints, IUTAM Prager Symposium on *Mechanics of Geomaterials: Rocks, Concretes, Soils*, (Edited by Z.P. Bažant), Northwestern University, Evanston, Illinois, 281–316.

Bažant, Z.P. (1984). Size effect in blunt fracture: Concrete, rock, metal. *Journal of Engineering Mechanics*, ASCE, **110**, 518–535.

Bažant, Z.P. (1987). Fracture energy of heterogeneous material and similitude. Preprints, *SEM-RILEM International Conference on Fracture of Concrete and Rock* (held in Houston, Texas, June 1987), (Edited by S.P. Shah and S.E. Swartz), publ. by SEM (Soc. for Exper. Mech.) 390–402.

Bažant, Z.P. (1997). Scaling of quasibrittle fracture: Asymptotic analysis. *International Journal of Fracture* **83**(1), 19–40.

Bažant, Z.P. (1998a). Modeling of compressive strain-softening, fracture and size effect in concrete. vol. 1 (*Proceedings of the EURO-C 1998 Conference on Composite Modelling of Concrete Structures* held at Badgastein, Austria, March 31–April 3, 1998), (Edited by R. de Borst, N. Bićanić, H. Mang, G. Meschke) publ. by A.A. Balkema Publishers, Rotterdam, Netherlands, 249–264.

Bažant, Z.P. (1998b). *Nonlocal Fracture Mechanics – Proposal of a new Approach to Nonlinear or Quasibrittle Fracture*. Preliminary Internal Report, Northwestern University, Dec.

Bažant, Z.P., and Cedolin, L. (1991). *Stability of Structures: Elastic, Inelastic, Fracture and Damage Theories*, Oxford University Press, New York.

Bažant, Z.P., and Chen, E.-P. (1997). Scaling of structural failure. *Applied Mechanics Reviews ASME* **50**(10), 593–627.

Bažant, Z.P., and Kazemi, M. T. (1990). Determination of fracture energy, process zone length and brittleness number from size effect, with application to rock and concrete. *International Journal of Fracture*, **44**, 111–131.

Bažant, Z.P., and Li, Z. (1995). Modulus of rupture: size effect due to fracture initiation in boundary layer. *Journal of Structural Engineering ASCE* **121**(4), 739–746.

Bažant, Z.P., and Li, Yuan-Neng (1995). Stability of cohesive crack model: Part II – Eigenvalue analysis of size effect on strength and ductility of structures. Trans. ASME, *Journal of Applied Mechanics* **62** (Dec.), 965–969.

Bažant, Z.P., Daniel, I.M., and Li, Zhengzhi (1996). Size effect and fracture characteristics of composite laminates. ASME Journal of Engineering. *Materials and Technology* **118**(3), 317–324.

Bažant, Z.P., and Zi, G. (1999). *Cohesive Crack Analysis of Kink Band Propagation and Size Effect in Fiber Composites*. Report, Dept. of Civil Engrg., Northwestern University, Evanston, Illinois – in preparation.

Budiansky, B. (1983). Micromechanics. *Computers and Structures* **16**(1–4), 3–12.

Budiansky, B. and Fleck, N.A. (1993). Compressive failure of fiber composites. *Journal of Mechanics and Physics of Solids* **41**(1), 183–211.

Budiansky, B., Fleck, N.A., and Amazigo, J.C. (1997). On kink-band propagation in fiber composites. *Journal of Mechanics and Physics of Solids* **46**(9), 1637–1635.

Christensen, R.M. and DeTeresa, S.J. (1997). The kink band mechanism for compressive failure of fiber composite materials. *Journal of Applied Mechanics ASME* **64** (March), 1–6.

Daniel, I.M., and Hsiao, H.M. (1996). Failure mechanisms in thick composites under compressive loading. *Composites, Part B*, **27B** 543–552.

Dempsey, J.P., Adamson, R.M., and Mulmule, S.V. (1995), Large-scale in-situ fracture of ice. vol. 1 (Procedings of 2nd International Conference on Fracture Mechanics of Concrete Structures (FraMCoS-2), held at ETH, Zürich), edited by F.H. Wittmann, Aedificatio Publishers, Freiburg, Germany 575–684.

Dempsey, J.P. et al. (1999). *International Journal of Fracture* (present Special Issue on Fracture Scaling, edited by Z.P. Bažant and Y.D.S. Rajapakse), in press.

Fleck, N.A. (1997). Compressive failure of fiber composites. *Advances in Applied Mechanics* **33**, 43–117.

Fleck, N.A., and Jelf, P.M. (1995). Deformation and failure of a carbon fibre composite under combined shear and transverse loading. *Acta Metallurgica Materialia* **43**(8), 3001–3007.

Fleck, N.A., and Shu, J.Y. (1995). Microbuckle initiation in fibre composites: a finite element study. *Journal of the Mechanics and Physics of Solids* **43**, 1887–1918.

Fleck, N.A., Sivashanker, S., and Sutcliffe, M.P.F. (1996). The propagation of a microbuckle in undirectional and multidirectional composites. *Acta Metallurgica Materialia*, submitted.

Fleck, N.A., Sivashanker, S., and Sutcliffe., M.P.F. (1997). Compressive failure of composites due to microbuckle growth. *European Journal of Mechanics A / Solids* 16, 65–82.

Fleck, N.A., Sutcliffe, M.P.F., Sivashanker, S., and Xin, X.J. (1996). Compressive R-curve of a carbon fibre-epoxy matrix composite. *Composites, Part B: Engineering* **27B**(6), 531–541.

Führing, H. (1973). Approximation functions for K-factors of cracks in notches. *International Journal of Fracture* **9**, 328–331.

G.R. Irwin, Fracture, in *Handbuch der Physik*, vol. VI, (Edited by W. Flügge), Springer Verlag, Berlin (1958) 551–590.

Jelf, P.M., and Fleck, N.A. (1992). Compression failure mechanisms in unidirectional composites. *Journal of Composite Materials* **26**(18), 2706–2726.

Kyriakides, S., Ascerulatne, R., Perry, E.J., and Liechti, K.M. (1995). On the compressive failure of fiber reinforced composites. *International Journal of Solids and Structures* **32**(6/7), 689–738.

Kyriakides, S., and Ruff, A.E. (1997). Aspects of failure and postfailure of fiber composites in compression. *Journal of Composite Materials* **31**(20), 2000–2037.

Moran, P.M., Liu, X.H. and Shih, C.F. (1995). Kink band formation and band broadening in fiber composites under compressive loading. *Acta Metallurgical Materialia* **43**(8), 2943–2958.

Newman, J.C. (1982). A nonlinear fracture mechanics approach to the growth of small cracks. *Proceedings, AGARD Conference on Behavior of Short Cracks on Airframe Components*, France.

Palmer, A., and Rice, J.R. (1973). The growth of slip surfaces in the progressive failure of over-consolidated clay. *Proceedings of the Royal Society of London* **A332**, 527–548.

Rice, J.R. (1968a). A path independent integral and the approximate analysis of strain concentrations by notches and cracks. *Journal of Applied Mechanics ASME* **35**, 379–386.

Rice, J.R. (1968b). Mathematical analysis in the mechanics of fracture. In *Fracture – an Advanced Treatise*, vol. 2, (Edited by H. Liebowitz), Academic Press, New York, 191–308.

Rosen, B.W. (1965). Mechanics of composite strengthening. *Fiber Composite Materials*, Am. Soc. for Metals Seminar, Chapter 3, American Society for Metals, Metals Park, Ohio, 37–75.

Schultheisz, C.R. , and Waas, A.M. (1996). Compressive failure of composites, part I: testing and micromechanical theories. *Progresive Aerospace Science* **32**, 1–42.

Soutis, C. and Fleck, N.A. (1990). Static compression failure of carbon fibre T800/924C composite plate with a single hole. *Journal of Composite Materials* **24**, 536–558.

Soutis, C., Fleck, N.A., and Smith, P.A. (1991). Failure prediction technique for compression loaded carbon fibre-epoxy laminate with open holes. *Journal of Composite Materials* **25** (Nov.), 1476–1497.

Soutis, C., Curtis, P.T., and Fleck, N.A. (1993). Compressive failure of notched fibre composites. *Proceedings of the Royal Society of London A* **440**, 241–256.

Sutcliffe, M.P.F., and Fleck, N.A. (1994). Microbuckle propagation in carbon fibre-epoxy composites. *Acta Metallurgica et Materialia* **42**(7), 2219–2231.

Sutcliffe. M.P.F., Fleck, N.A., and Xin, X.J. (1996). Prediction of compressive toughness for fibre composites. *Proceedings of the Royal Society of London*, Series **A452**, 2443–2465.

Tada, H., Paris, P.C. and Irwin, G.R. (1985), *The Stress Analysis of Cracks Handbook*, Del Research Corp., Hellertown, PA.

Waas, A.M., and Schultheisz, C.R., (1996). Compressive failure of composites, part II: experimental studies. *Progressive of Aerospace Science* **32**, 43–78.

Zi, Goangseup (1998). Note privately communicated to Z.P. Bažant on Nov. 13.